Non-invasive hemoglobin sensing and imaging: optical tools for disease diagnosis

Michaela Taylor-Williams,[1,2] Graham Spicer,[1,2] Gemma Bale,[1,3] and Sarah E Bohndiek[1,2*]

[1] Department of Physics, Cavendish Laboratory, University of Cambridge, JJ Thomson Avenue, Cambridge, CB3 0HE, UK

[2] Cancer Research UK Cambridge Institute, University of Cambridge, Robinson Way, Cambridge, CB2 0RE, UK

[3] Department of Engineering, Electrical Division, University of Cambridge, 9 JJ Thomson Avenue, Cambridge, CB3 0FA

* Address correspondence to: Sarah E Bohndiek, Department of Physics, Cavendish Laboratory, University of Cambridge, JJ Thomson Avenue, Cambridge, CB3 0HE, UK and Cancer Research UK Cambridge Institute, University of Cambridge, Robinson Way, Cambridge, CB2 0RE, UK; email seb53@cam.ac.uk ; phone +441223 337267.

Abstract

Significance: Measurement and imaging of hemoglobin oxygenation is used extensively in the detection and diagnosis of disease, however, the applied instruments vary widely in their: depth of imaging; spatiotemporal resolution; sensitivity; accuracy; complexity; physical size; and cost. The wide variation in available instrumentation can make it challenging for end users to select the appropriate tools for their application and to understand the relative limitations of different methods.

Aim: To provide a systematic overview of the field of hemoglobin imaging and sensing.

Approach: We reviewed the sensing and imaging methods used to analyse hemoglobin oxygenation, including: pulse oximetry; spectral reflectance imaging; diffuse optical imaging; spectroscopic optical coherence tomography; photoacoustic imaging; and diffuse correlation spectroscopy.

Results: We compare and contrast the ability of different methods to determine hemoglobin biomarkers such as oxygenation while considering factors that influence their practical application.

Conclusions: We highlight key limitations in the current state-of-the-art and make suggestions for routes to advance the clinical use and interpretation of hemoglobin oxygenation information.

Keywords Hemoglobin; sensing; imaging; spectroscopy.

1. Introduction

Optical-imaging biomarkers are defined characteristics measured with an optical imaging modality to indicate normal biological or pathological processes. Optical-imaging biomarkers can help researchers better understand disease development and give clinicians the ability to diagnose and treat diseases in patients.[1,2]

Based on the absorption of light by hemoglobin, optical-imaging biomarkers such as hemoglobin concentration, oxygen saturation, and blood flow can be measured with a range of instruments for clinical disease evaluation. Hemoglobin is a protein in blood that transports oxygen to organs. Oxygen plays a vital role in cells aerobic respiration, where it reacts with glucose to form adenosine triphosphate (ATP), water (H_2O), and carbon dioxide (CO_2), which is essential for maintaining healthy tissue and blood vessels. Hemoglobin oxygenation is often used as a vital sign; low oxygenation at the level of the organism can indicate a systemic disease, such as chronic obstructive pulmonary disease, apnea.[3,4] Poor oxygenation in a particular organ or tissue can be symptomatic of an insult due to injury or illness, such as diabetes, skin trauma, rheumatic disease or cancer.[1,5–8]

Non-invasive, low-cost, safe and portable methods based on optics for extracting hemoglobin-derived biomarkers have become vital tools in patient management that can be applied in real-time at the bedside. Despite widespread use of methods such as pulse oximetry, the uptake of newer technologies that go beyond point measurements remains relatively limited, however, there are many promising tools in development, ranging from 3D volumetric imaging of vascular architecture to spatially-resolved functional images of tissue oxygenation. Being less expensive and more portable in general than conventional radiological imaging methods, these have the potential to impact patient care in a wide range of debilitating illnesses, ranging from rheumatoid and vascular diseases, to neurodegenerative diseases and cancer.

Here, we review these non-invasive methods for quantifying hemoglobin-derived biomarkers, including pulse oximetry, as commonly used in clinical practice worldwide, together with promising tools emerging in the research setting for imaging. The relative strengths and weaknesses of different methods are considered according to the application, grouped by mode of operation: single-point detection; superficial imaging (up to 1-2 mm depth); and deep tissue imaging. We compare techniques based on the technology used, analysis methods, and current research or clinical applications, before highlighting limitations that would benefit from future research.

2. The Impact of Tissue Properties on Optical Measurement of Hemoglobin Biomarkers

The biology of human blood

Human blood consists of plasma (about 55 vol%) and cells (approximately 45 vol%) where 99% of the cells are red blood cells (RBCs), and the remaining 1% are leukocytes and thrombocytes.[9,10] Plasma is a complex composition of dissolved ions (electrolytes), lipids, sugars, and proteins.[10] RBCs, also known as erythrocytes, have a flat biconcave shape, a mean volume of 90 μm^3 [9,11] and contain about 30 pg of hemoglobin, a globular metalloprotein responsible for oxygen transport throughout the body.[9,11] Hemoglobin concentrations range from 134 to 173 g/L in whole blood and 299 to 357 g/L in RBCs, according to age, gender, and health status. For example, anaemia, cancer, or hereditary hemochromatosis, decrease hemoglobin levels in the blood.[9,12]

Each hemoglobin molecule contains four heme groups that can be bound to oxygen; the unbound state is referred to as deoxygenated hemoglobin, Hb, while the saturated bound state is considered oxygenated and denoted by HbO_2.[10] Sometimes the oxygen saturation of arterial blood, SaO_2, is differentiated from that of peripheral blood, StO_2, since arterial blood

oxygenation should be the same throughout the body. In contrast, peripheral blood will have varying oxygenation levels as oxygen is absorbed from the blood by peripheral systems.[11,13,14] Hemoglobin is also able to bind to other molecules forming: carboxyhemoglobin, which arises during carbon monoxide inhalation;[15,16] sulfhemoglobin, which arises due to the irreversible binding of sulphur in the presence of sulfonamides;[17] and carbaminohemoglobin, which results from binding of hemoglobin in venous blood to carbon dioxide.[18] A further variant state of hemoglobin is methemoglobin,[19–21] where hemoglobin binds iron in the Fe^{3+} state (unlike normal hemoglobin that binds Fe^{2+}) which prevents binding of oxygen. Methemoglobin occurs naturally in blood at ~1-2% concentration[15] but can be elevated due to side effects of medication, or environmental factors.[22] Finally, genetic variants of hemoglobin, such as hemoglobin S, which causes sickle cell anaemia, can influence hemoglobin structure and binding properties.[23] Myoglobin, a chromophore commonly found in muscles, binds oxygen with a higher affinity than hemoglobin.[24] Myoglobin has a similar spectral response to hemoglobin, and may be found in the bloodstream following muscle injury.[24,25]

Optical properties of biological tissue

Tissue is a complex turbid medium composed of different cell types and protein-rich extracellular matrix, which strongly impact the propagation of light.[11,26,27] Absorption is the transformation of light energy to some other form of energy, such as heat, sound or fluorescence, as light traverses tissue, quantified by the absorption coefficient, μ_a [cm^{-1}]. Absorption is the primary optical interaction that is exploited to measure hemoglobin biomarkers. In turbid media, scattering is a major contributor to light attenuation and can confound attempts to measure hemoglobin absorption, since blood is a highly ing liquid with strong anisotropy. Scattering refers to a change in the direction of light propagation and is quantified by the scattering coefficient, μ_s [cm^{-1}], together with directional factors such as the

scattering phase function and anisotropy factor, which further relate to the tissue refractive index.

Optical properties of RBCs, hemoglobin, and its derivatives

The absorption coefficient of hemoglobin is a function of wavelength and the binding state (Fig. 1).[28] While hemoglobin is usually oxygen bound, other variants mentioned above can modify the absorption spectrum and should be considered if relevant to the pathology being assessed since they can confound the measurement.[10,13,23,29,30] It should be noted that the spectra of hemoglobin and its variety of physiologically relevant bound states are often measured after extracting the hemoglobin protein from RBCs, so they do not consider variation that arises due to scattering from different RBC geometries and orientations.

In the absence of shear stress, human RBCs are biconcave discs with a diameter of 7-8 μm, maximal thickness of 2-3 μm, and minimal thickness of 0.8-1.5 μm[31,32]. Concentrations of Hb within an RBC are high, on the order of 300-360 mg/mL, and the total refractive index of the cell is well approximated by that of pure hemoglobin through application of the Kramers-Kronig relations on the total absorption spectrum[33,34]. When light is incident upon a single RBC, scatter from the near and far membrane interfaces leads to a characteristic oscillatory scattering spectrum and phase function[32,35]. The oscillatory spectral shape makes oximetry of a single RBC impossible without *a priori* knowledge of the precise shape and orientation of the RBC, however, averaging over many cells with random orientation can smooth this oscillation, which permits measurement of oxygen saturation of RBCs in capillaries[35,36]. In addition, hematocrit, the volume fraction of RBCs in whole blood, the presence of blood plasma, and other factors affect the absorption spectra.[18,37–40]

The most common hemoglobin-derived optical-imaging biomarkers are total hemoglobin (referred to as THb hereafter) and oxygen saturation (referred to as sO_2 hereafter). THb is often evaluated using a single wavelength absorption measurement taken at an isosbestic point of HbO_2 and Hb (i.e. when their absorption coefficients are equal). sO_2 requires an absorption measurement to be made at multiple wavelengths (at least 2), usually spanning regions where either HbO_2 and Hb dominate the absorption properties. Data are then often analysed by applying multivariate statistical approaches for spectral unmixing[41] to extract the sO_2 value. The absorption coefficients of HbO_2 and Hb are related through sO_2 to the overall optical absorption μ_a by the equations;[11,41]

$$sO_2 = \frac{[HbO_2]}{[HbO_2] + [Hb]} \tag{1}$$

$$\mu_a(\lambda) = c_{Hb} \left\{ \frac{\mathrm{sO_2}}{100} \mu_{aHbO_2}(\lambda) + \left(1 - \frac{\mathrm{sO_2}}{100}\right) \mu_{aHb}(\lambda) \right\} \tag{2}$$

where c_{Hb} is the concentration of hemoglobin in the tissue.

In addition to hemoglobin, many other molecules interact with light depending on their concentration and distribution throughout the tissue,[42] which can disrupt light propagation and also introduce spectral coloring at depth in tissue, confounding attempts to measure THb and sO_2. Furthermore, the scattering and refractive index properties of blood are affected by hemoglobin concentration, erythrocyte volume, shape and aggregation, each of which can be modified in disease. Unlike the absorption coefficient, the anisotropy and the scattering coefficients of blood are not dependent on the changes in oxygenation.[9,43]

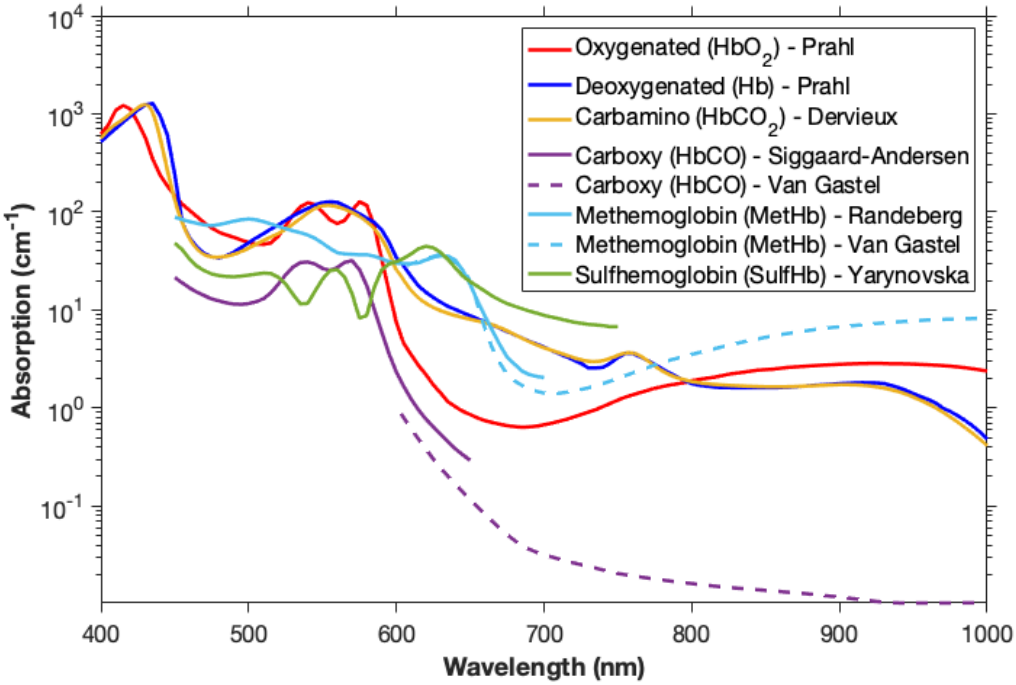

147

148 **Fig. 1: The optical absorption of hemoglobin and associated variants.** Representative spectra are shown
149 for oxygenated,[44] deoxygenated,[44] carbamino,[18] carboxy (visible[45] and NIR[19,20]), methemoglobin (visible[46]
150 and NIR[19,20]), and sulfhemoglobin.[47]

151 While hemoglobin-derived biomarkers often rely on variations in the absorption or
152 scattering by hemoglobin molecules or RBCs, the hardware used to make these measurements
153 varies, including the use of LEDs or lasers for illumination with optical sensors (both arrays
154 and point sensors) or ultrasound sensors for detection. The methods described in this review
155 are summarized in Table 1.

156

3: Point Sensing of Hemoglobin sO_2 through Pulse Oximetry

Pulse oximetry makes a localised measurement of arterial hemoglobin sO_2. To make this measurement, the absorption of tissue is evaluated at two or more different wavelengths, selected according to where the absorption coefficients of Hb and HbO_2 differ sufficiently for their ratio to be evaluated as a biomarker that can be correlated directly to sO_2 (Equation 1).

Clinical Applications and Research Studies

Pulse oximetry has been extensively reviewed elsewhere.[13,48–51] Pulse oximetry is deployed in many medical applications, from at-home first aid to clinical intensive care units and surgical theatres[13] and has found particular utility to assess hypoxemia in COVID-19 patients[52] as non-specialists with minimal training can efficiently operate pulse oximeters.[51,53] Pulse oximetry research in the clinic focuses on its use in treating and diagnosing diseases, such as optimizing oxygenation of ventilated patients, screening neonates for congenital heart diseases, and monitoring patients with sleep apnoeas.[54–57] Despite widespread use, it is also well established that pulse oximetry can suffer racial bias, which results in less accurate oxygenation readings for patients with more skin melanin content, a trait associated with darker skin. The impact of such bias is severe as it has been shown to result in less adequate medical treatment of such patients, meaning it is important for clinicians to be aware of this limitation and it is also an important area for future research and development.[58,59] While this bias has been well known for some time, it has been increasingly studied as a result of COVID-19 and the increased clinical use of pulse oximeters to treat respiratory conditions.

Technology

Light absorption in pulse oximetry is typically measured using alternating illumination by LEDs at two different wavelengths.[49,60,61] Since the wavelength of the illuminating light is altered with time, oxygenation measurements are susceptible to motion artefacts, which change the area of tissue being illuminated and coupling to the tissue, resulting in inaccuracies. Commonly used wavelength pairs are 660 nm and 940 nm, or 665 nm and 894 nm,[13,62–65] applied in two different modes:

- Transmission: Tissue such as the finger, toe, or earlobe is illuminated, and the light transmitted through the tissue is detected by a sensor to determine the amount of light attenuated by the tissue (Fig. 2a).
- Reflection: Tissue such as the finger, foot, or forehead is illuminated, and the amount of light reflected by the tissue and underlying bone is detected by a sensor and used to determine the amount of light that the tissue has absorbed. Reflection pulse oximetry tends to have a higher signal when there is low perfusion.[13,66] In reflection pulse oximetry, it can be challenging to isolate the light that has gone deeper into tissue from light that has been scattered or reflected at the surface of the tissue (Fig. 2b).

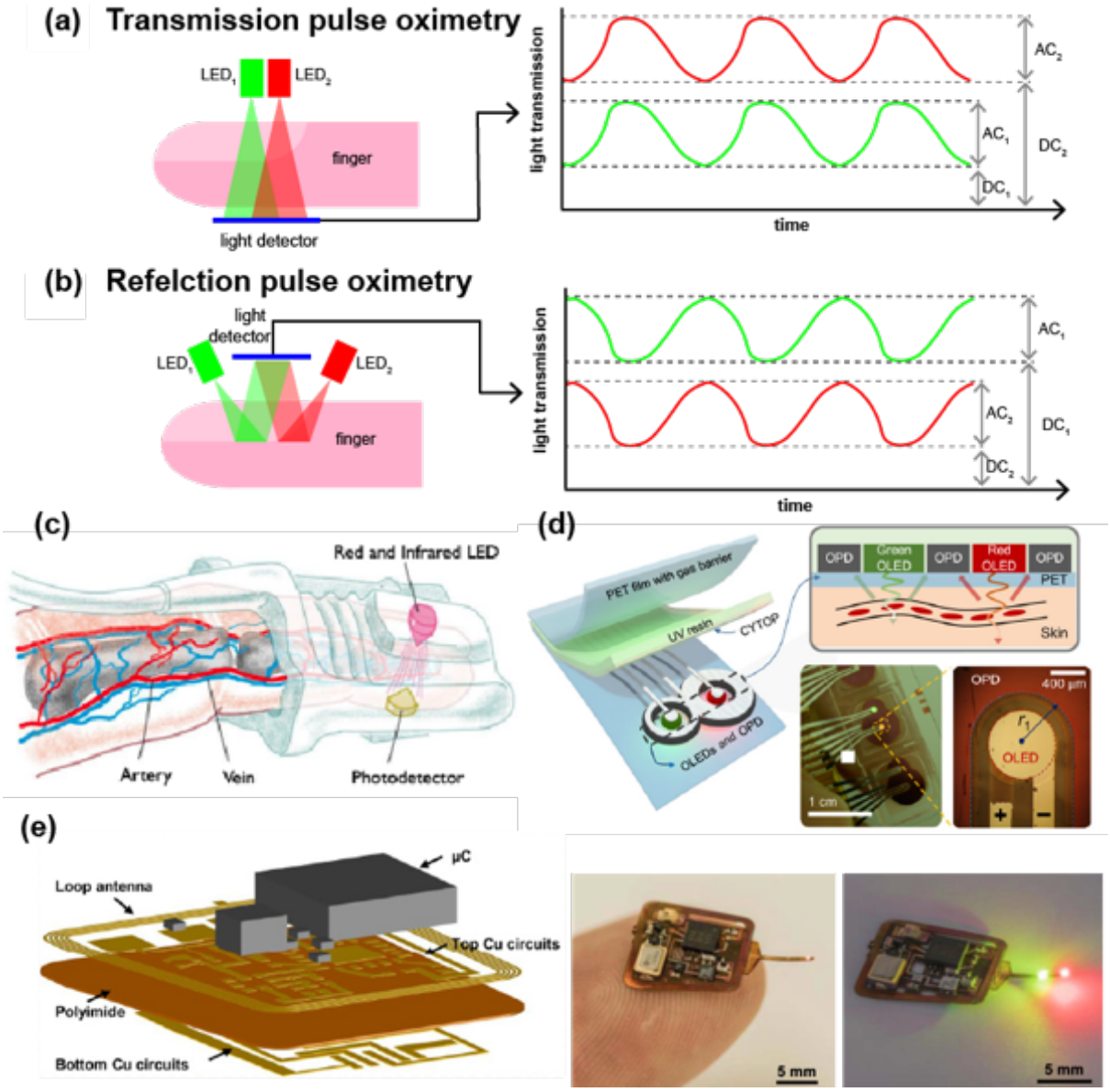

Fig. 2: Pulse oximetry. Schematic illustration of pulse oximetry in the two different operation modes (a) reflection and (b) transmission. The detected light is cyclic due to the pulsatile nature of blood in the peripheral vascular system. Both transmission and reflection modes have alternating components (AC) and direct components (DC). In tissue, the transmission and reflection of light vary based on the changes in absorption due to blood volume and oxygenation. That is $\mathbf{R + A + T \approx 1}$, when R, A, and T are the normalized reflection, absorption, and transmission intensities. For this reason, in reflection pulse oximetry, the peak intensity of light will be off by half a cycle from that of the transmission cycle. Examples of pulse oximeter devices include: (c) transmission-based devices widely used in a clinical setting;[67] (d) low-power devices in development that adhere to the skin and use flexible OLED illumination;[57] (e) battery-free pulse oximeters in development that use near field communication for power.[68]

Evolving from the traditional fingertip pulse oximeters (Fig. 2c), the current development of the technology mainly targets wearable devices and focuses on: low power usage (Fig. 2d); optimization of signal detection; reduction of motion artefacts; flexible illumination and detection (Fig. 2e); low-cost devices; miniaturization; and calibration techniques.[57,69–72]

Analysis

The theory of oximetry analysis has been extensively reviewed by Mackenzie & Harvey,[73] so it will be only briefly introduced; readers are referred to the prior review for a more detailed description. The total extinction coefficient for blood is denoted as ε and related to SaO_2 by the equation:[13]

$$\varepsilon = \varepsilon_O \, SaO_2 + \varepsilon_D \, (1 - SaO_2). \tag{3}$$

Further analysis of the extinction coefficient is needed to isolate the signal from arterial blood since venous blood also absorbs the light, along with other chromophores that appear in the light path, such as melanin (in the skin). It is possible to exploit the cyclic nature of the extinction coefficient due to the pumping of blood, finding the ratio of the variable component (AC) and constant component (DC) at two different wavelengths (Fig. 2a,b), where the difference in light absorption is rather large:[13,48,49]

$$R = \frac{(AC/DC)_1}{(AC/DC)_2} \tag{4}$$

The ratio R, also known as the modulation ratio, is then related to SaO_2 through a calibration procedure using best fit analysis according to the equation:

$$SaO_2 = a + bR \quad (5)$$

where the variables *a,* and *b* are calculated for each device during testing, based on a linear regression between the modulation ratio and the SaO_2 value.[49,74] Calibration was originally performed with human volunteers, changing SaO_2 values by limiting the oxygen in the air they breathed from 70% to 100% SaO_2, which determined R values.[75] These are valid across devices with the same design, which meant individual devices did not have to be calibrated. Calibration techniques have evolved, so volunteers are no longer required. For example, several devices simulate the circulatory system and finger using pumps to mimic the pulsatile flow of arterial blood and venous blood.[12,76–80] The system is then sealed off, and the oxygenation of the blood can be controlled by varying the oxygen content of the system. Alternatives include electrical simulators that emit light from an LED corresponding to the light detected by the sensor to mimic the light transmitted in a typical finger. This technique requires prior knowledge of the pulse oximeter being calibrated. Once in operation, pulse oximeters are rarely recalibrated.[75]

Limitations

Pulse oximetry measurements typically have an error of 3-4% depending on the device and calibration used, which is actually sufficient to impact patient care in some cases.[75,81] In addition, standard pulse oximeters cannot detect the presence of methemoglobin, carboxyhemoglobin, or hemoglobin mutations, although their presence and concentrations outside of the expected range will affect the oxygenation readings.[15,23] Some targeted pulse oximeters are able to detect methemoglobin and carboxyhemoglobin, but they are usually used in specific scenarios where high levels of these derivatives are expected due to exposure.[82] Hemoglobin F, present in foetuses and infants under 6 months, has a greater oxygen affinity, which allows the foetus to absorb oxygen from the mother's bloodstream;[10] in infants, its

presence can increase the error in pulse oximetry by a further 3% in addition to the typical errors.[13] Additionally, when there is poor perfusion to tissues, pulse oximetry can be limited, and if there is not a significant pulse detected, the technique will have increased inaccuracies.[65] Finally, pulse oximetry has been found to suffer racial bias in two large cohorts, where black patients had nearly three times the frequency of occult hypoxemia not detected by pulse oximetry as white patients.[58,59] Skin pigmentation leads to an overestimation of arterial oxygen saturation in dark-skinned individuals, which could seriously impact medical decision making and long-term outcomes.[83] These limitations merit increased attention in research and development given the potential for long-term and widespread use of pulse oximetry in COVID-19 patient management and the interest in deployment of the technology in the wearable setting.

4: Reflectance Imaging of Hemoglobin

Optical imaging of hemoglobin biomarkers requires the operator to build up a spatially resolved map of hemoglobin absorption at multiple wavelengths, again exploiting the differential absorption coefficients of Hb and HbO_2.[26,84,85] Several methods can be used to achieve this, including: point-scanning spectroscopy; multispectral imaging; and hyperspectral imaging (Fig. 3a). The result is a 3D dataset (x,y,λ)[26,85–87] that can be subjected to multivariate analysis methods to extract from the measured spectra the concentrations of their contributing chromophores (e.g. Hb and HbO_2), referred to as 'endmembers' for unmixing.[26,87–91] From these multivariate analyses, biomarkers that relate to THb and sO_2 can then be extracted.

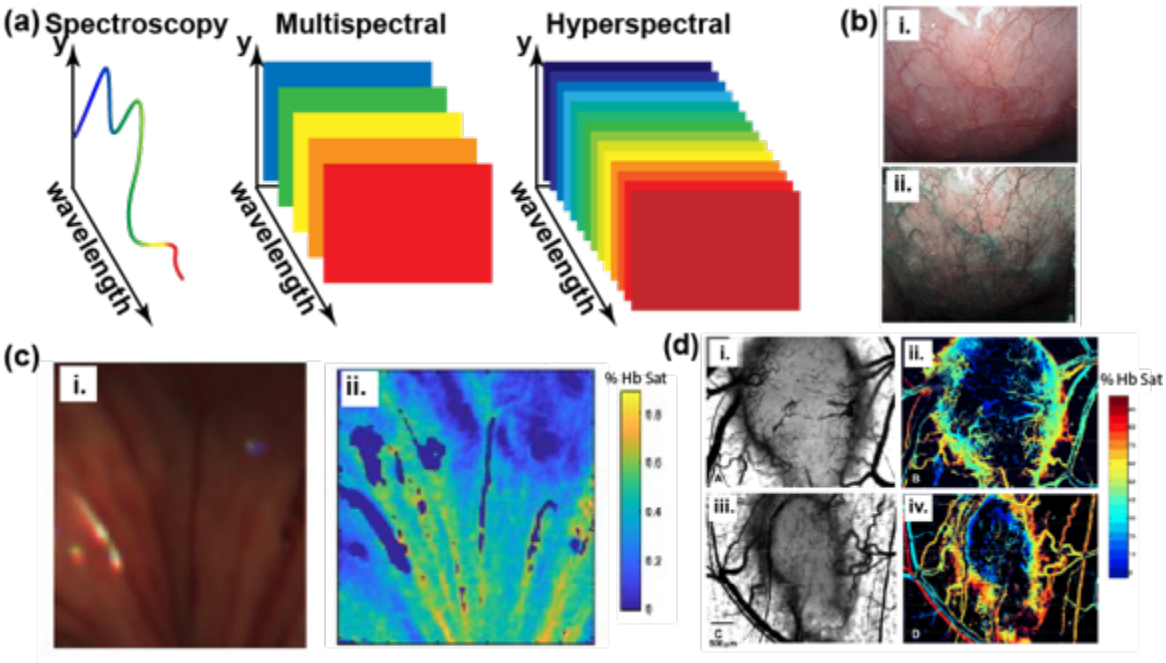

Fig. 3: Spectral reflectance imaging. (a) Overview of spectral reflectance imaging methods.[85] Point-scanning spectroscopy can be used to build up spectral information using a standard spectrometer. Alternatively, a spectral camera can be used, which either collects a limited number of wavelengths (multispectral, typically < 10 spectral bands) or a more continuous spectrum (hyperspectral). (b) Endoscopy images of the oesophagus with (i) RGB imaging and (ii) narrowband imaging, that improves the contrast of the blood vessels.[92] (c) Endoscopy of a porcine oesophagus to determine tissue viability with 24 spectral bands from 460 to 690 nm (spectral resolution of 10 nm) using a slit hyperspectral imaging and fibre bundle probe and the resulting (i) reconstructed RGB image, and (ii) unmixed oxygenation.[93] (d) Hypoxia of tumous can be imaged using a liquid crystal tuneable filter in conjunction with a CCD; this is demonstrated in mouse tumors (i) and (iii) show light microscopy of tumor vasculature in a dorsal skin window chamber, the additional information of haemoglobin saturation is shown in (ii) and (iv) illustrating low oxygen saturation of the tumors.[94]

Clinical Applications and Research Studies

A widespread application of reflectance hemoglobin imaging is in gastrointestinal endoscopy. Virtual chromoendoscopy methods adapt the light source of the endoscopy to focus on two wavelength bands (415 and 540 nm), where hemoglobin absorbs strongly (Fig. 1), thus providing a high contrast morphological image of the tissue vasculature to the clinician.[2,95] Narrowband imaging is the most widely established of these methods and meets the ASGE thresholds for targeting biopsies when imaging patients with Barrett's esophagus for early signs of cancer.[96] More recently, clinical research studies have demonstrated that by expanding the

number of wavelengths captured in endoscopy,[87,97,98] it is possible to derive hemoglobin biomarkers of THb and sO_2 from spectral information to classify disease status,[99] however, further clinical study is needed to demonstrate efficacy.

Capillaroscopy is another reflectance-based imaging technique, used to image the blood vessels in the finger nailfold to diagnose disease, particularly to identify rheumatic diseases such as systemic scleroderma. Capillaries are micro blood vessels from which oxygen and other nutrients are exchanged with the surrounding cells. In the finger nailfold, the capillaries are oriented in loops parallel to the skin, allowing full visualisation at high resolution in reflectance imaging mode. While capillary walls, formed from a single layer of endothelial cells lining the vessels, can rarely be detected during capillaroscopy, the RBC column is visible and morphological features associated with the capillary can be measured using monochrome, narrowband, and RGB imaging.[100] Capillary blood flow in the finger ranges in velocity from 0.67-4 mm/s depending on physiological factors and the cyclic nature of perfusion.[101–103] Morphological dysfunction of the capillaries is easily identified using the current techniques, but current methods do not make oximetry measurements related to this dysfunction.

Reflectance-based oximetry imaging has been widely explored in retinal imaging since the retina is one of the most metabolically active tissues in the human body.[104] Commercial retinal oximeters are applied to fundus cameras and use dual-wavelength illumination, akin to pulse oximetry, to acquire images simultaneously at one isosbestic wavelength and one sensitive to HbO_2. Abnormal retinal oxygenation has been shown to detect diabetic retinopathy, age-related macular degeneration, and glaucoma.[105–107] In addition, the retina has similar vascular properties to the brain, making it a perfect window to understand and diagnose neurological disease in addition to ocular disease.[106] Nonetheless, retinal oximetry has yet to find routine clinical application, limited primarily by the impact of fundus pigmentation and

vessel size on quantification.[106] While some hyperspectral imaging technologies have been explored in an attempt to overcome these limitations, to the best of our knowledge, they have not found clinical application.

In smaller scale studies, clinical trials of reflectance-based hemoglobin imaging have been applied in areas from the skin to the brain. For example, the hemodynamic response of the human cortex has been visualised during open-cranium surgery using hyperspectral imaging combined with multivariate analysis.[108] Evaluation of hemoglobin oxygenation and melanin content in the face has been of interest for dermatological treatments such as detection of skin cancer, assessment of scar healing and evaluation of skin thickness.[109–112] Spectral imaging of hemoglobin in burns,[8] wounds,[6] and bruises[46,113] has been explored to assess the progress of healing in a quantitative manner. Moreover, spectral imaging of tissue sO_2 has found application in intraoperative imaging.[93,114] Post-operative imaging can also provide clinicians with information on how tissue is healing such as following breast reconstruction where water, haemoglobin concentration, and oxygen saturation are key indicators for tissue perfusion, an important factor in recovery.[115]

Technology

The simplest imaging oximetry methods include 2 or 3 wavelengths akin to pulse oximetry, which can be applied using sequential illumination by the target wavelength bands and imaging with a single camera, or simultaneous illumination of all wavelengths (e.g. with broadband illumination) and capture using a spectrally resolved method, such as image splitting through band pass filters applied in front of two cameras. Expanding the spectral range of wavelengths to capture more spectral features of Hb or HbO_2 (in the visible but also near-infrared range[116]) requires more complex hardware.

There are three main types of multi or hyperspectral systems used in medical imaging that can be applied for unmixing oxygenation of tissue.[85,117,118] In spatial scanning, a spectrograph records the spectral dimension (λ) while being scanned across a sample. A 1D spectrograph may be point-scanned or a 2D spectrograph may be line scanned. The approach sacrifices temporal resolution and hence requires minimal movement of the sample to avoid motion artefacts. In spectral scanning, a 2D camera records the spatial dimensions (x,y), while the spectral dimension is scanned, for example, by changing the illumination wavelength or by filtering the imaging light path (e.g. with a filter wheel or tunable filter). This also has a scanning time associated with it so requires minimal movement to prevent spectral artefacts.

Finally, in snapshot methods, a system outputs spectral and spatial dimensions (x,y,λ) simultaneously without scanning.[117,118] Snapshot systems may use beam splitting with dichroic filters, volume holographic optical element splitters, image replicating spectrometers, or multispectral filter arrays in the imaging path. Snapshot methods avoid motion artefacts, which makes them an exciting prospect for clinical application, however, often exhibit poor optical efficiency. They also require a trade-off between spatial and spectral resolution, although this is less problematic for hemoglobin measurements, where the target spectra are well characterized, and extensive evidence exists for the application of optical measurements. Nonetheless, optimization of the target wavelengths for snapshot imagers can substantially improve their performance.[90,119–122]

In addition to these intensity-based imaging methods, spatial frequency domain imaging (SFDI) can be used to interrogate hemoglobin-related biomarkers by exploiting modulated illumination of the tissue. SFDI typically uses sinusoidal patterns and extracts the demodulation of these patterns reflected from tissue to calculate absorption and scattering properties; [123,124] low frequencies are more sensitive to absorption while high frequencies are

more sensitive to scattering.[124] Multiwavelength illumination[125] can then be used to calculate hemoglobin content and oxygenation,[126,127] for example, in monitoring of peripheral circulation and vascular diseases,[128] for which there are FDA-cleared devices, as well as ulcers,[129] burns,[130] or tumor margin detection.[131,132] SFDI provides relatively high-resolution images, but conventional methods can be sensitive to motion artefacts[123] and computational processing can limit the rate of image display. More recent reports have shown that it is possible to overcome these limitations using single snapshot of optical properties (SSOP) methods, which can achieve video-rate imaging.[133]

Analysis

Two or three wavelength imaging methods may be viewed qualitatively and interpreted by the operator, as in narrowband imaging, or processed to output quantitative THb or sO_2 biomarkers in a manner similar to pulse oximetry, through calculation of image ratios and calibration of the results. For spectral imaging methods, analysis can be time-intensive due to the large amount of data collected, which can be problematic for clinical translation where the real-time display of biomarker data is often desired. Analysis methods vary depending on the biomarkers targeted and the type of tissue imaged from the simplest techniques, linear spectral unmixing,[134,135] to more complex methods such as multivariate analysis and machine learning.[26,87–89] Linear spectral unmixing determines the type and concentration of chromophores present based on input reference spectra for oxy and deoxy hemoglobin, from which oxygen saturation can be calculated.[97,108,136,137] Spectral signatures can also be used directly in classification of disease status, for example, cancer.[99,114,138,139] Sometimes, a combination of classification and unmixing techniques can produce the optimal results, allowing for data corrections to be applied in certain tissue types.[26,90,97,108] Similar methods are

also used in depth-resolved imaging, but data may need to be corrected based on the imaging depth and the associated level of optical absorption and scattering. Machine learning methods have shown promise in this regard, enabling more accurate determination of hemoglobin oxygenation, particularly at depth, than classic linear spectral unmixing.[140]

Limitations

Imaging tools for the assessment of hemoglobin can be subject to the same limitations as pulse oximetry. In addition, constraints that presently prevent clinical adoption of reflectance-based spectral imaging include: cost; reliability of THb and sO_2 measurements; clinical evidence for sensitivity and specificity of THb and sO2 in the diseases shown to be of interest in small scale studies; and the need to process data in real-time.[2,84,91] These challenges are common in the clinical translation of optical-imaging biomarkers,[2] though fortunately, in the case of hemoglobin biomarkers, many devices have already navigated the pathway to the clinic, enabling initial studies to be undertaken.

5: Depth-resolved Imaging

A key limitation with pulse oximetry and reflectance-based imaging is their inability to provide depth-resolved imaging of hemoglobin biomarkers. Two modalities are available to determine THb and sO_2 in tissue up to and beyond depths of 1 cm: Photoacoustic Imaging (PAI) and Diffuse Optical Imaging (DOI); both have been evaluated in clinical trials and are at different stages of clinical adoption. PAI exploits the generation of acoustic waves by the absorption of pulsed light by hemoglobin to create deep tissue volumetric maps using pulsed illumination and ultrasound detectors (Fig. 4a).[141–143] DOI measures the properties of light scattering in tissue to generate absorption maps using synchronized illumination and photodiode-based detection (Fig. 4b).[144–146] At more restricted depths, below 1 cm,

spectroscopic optical coherence tomography (OCT) is also applicable, combining broadband illumination with spectrally-resolved interferometric detection. While these methods have been widely explored in the clinical research setting, they are only just beginning to find routine application in the clinic for patient management.

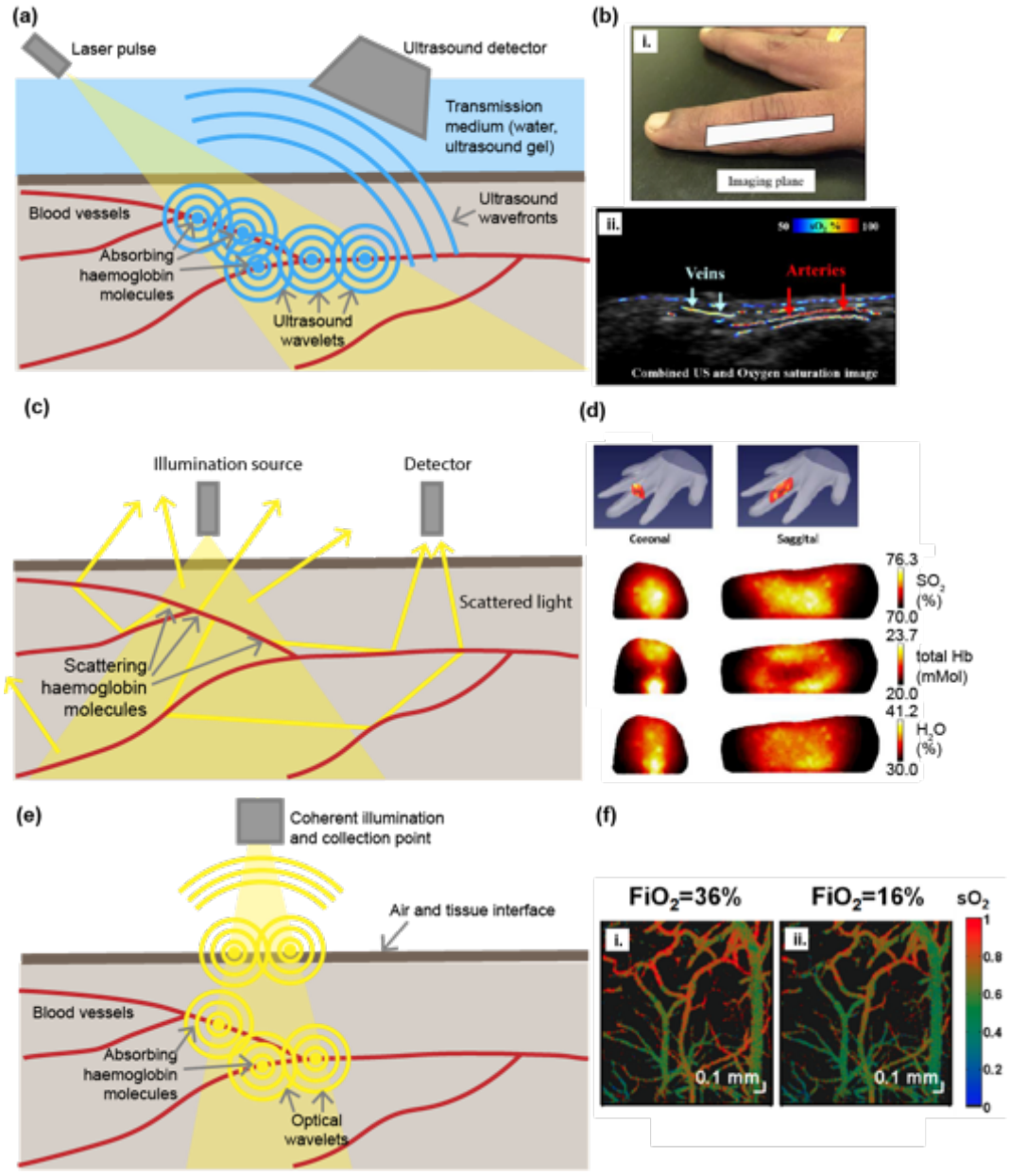

Fig. 4: Principles of depth-resolved imaging. (a) In photoacoustic imaging, the absorption of light pulses generates a broadband acoustic wave detected at the tissue surface by an ultrasound transducer. (b) Photoacoustic imaging of oxygenation of the finger in combination with ultrasound to image the veins and arteries.[147] (c) In diffuse optical imaging (and diffuse

correlation spectroscopy techniques), illuminated light is scattered in tissue collected by an offset optical detector at the tissue surface. (d) DOI data acquired from the human finger, processed to quantify oxygenation, hemoglobin concentration, and water.[148] (e) In OCT coherent light illuminates the tissue and the light that reflects at interfaces is collected and combined with a reference arm, so interference occurs; from this interference, depth resolved images of the absorption and scattering properties of tissue can be resolved. (f) Oxygen resolved spectroscopic OCT on mice brains illustrating how the fraction of inspired oxygen (FiO_2) affects the oxygenation of the arteries and veins in the brain.[149]

5.1 Photoacoustic Imaging (PAI)

Clinical research studies

By far, the most explored clinical PAI application is human breast cancer detection, extensively reviewed elsewhere,[150,151] due to the enhanced angiogenesis of breast cancers compared to background breast parenchyma and the scalability of PAI geometry allowing a broad view of the area (Fig. 5a).[141,150–154] Multicentre clinical trials have recently been concluded covering more than 2000 women, which established the ability of PAI to increase the specificity of ultrasound imaging using a real-time map of relative Hb and HbO_2.[152,155] PAI has also been explored in other cancer types, considering that neoangiogenesis is a hallmark of cancer, including thyroid,[156] prostate,[155] and melanoma among others.[157] Beyond applications in cancer, PAI has found a wide range of potential applications where depth-resolved information is required, for example: in endoscopic procedures;[158,159] for evaluation of inflammation, such as arthritic joints,[143,160] foot ulcers,[161] and Crohn's disease;[162] vascular imaging;[163] and for the guidance of interventional procedures, such as in fetal placentas.[164]

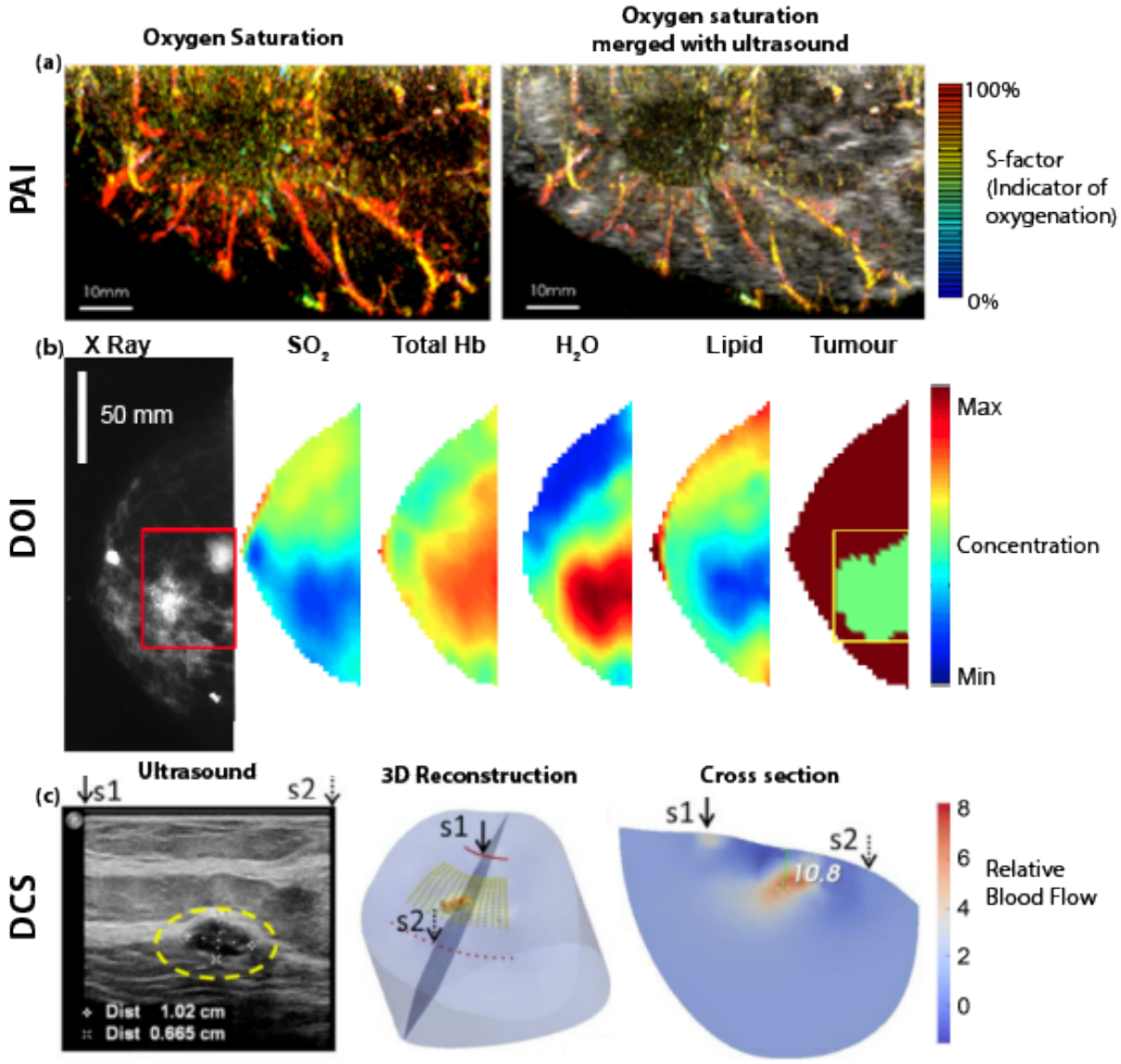

Fig. 5: Tomographic imaging of the human breast for cancer detection (a) PAI of sO_2 in a breast with infiltrating ductal carcinoma (IDC); S-factor was defined to account for system accuracy and fluence compensation.[165] (b) DOI of breast IDC (indicated by the red box) resolves sO_2, THb, H_2O, Lipid, concentrations of which serve to highlight the tumor.[166] (c) Diffuse correlation spectroscopy (DCS) of blood flow relative to an ultrasound image of low-grade carcinoma where the tumor is circled in yellow. These images are referenced to positions s1 and s2 to compare the ultrasound, 3D reconstruction, and cross section.[167]

Technology

Pulsed illumination is required to excite PAI signals. Typically, tunable pulsed lasers with nanosecond pulse durations have been used, however, pulsed laser diodes and LEDs have

emerged recently as viable alternatives.[168] The generated acoustic waves are detected by ultrasound transducers, which may be single-element, linear or curvilinear arrays or in a spherical arrangement, depending on the system's geometry. The type of transducer and associated center frequency or bandwidth are usually governed by the application, depending on the absorber size, laser pulse width and required imaging depth.[169] PAI can be deployed in different geometries, including tomography, mesoscopy and microscopy. Tomography systems have found the most widespread clinical application as they provide an adequate field of view and spatial resolution for imaging of hemoglobin in deep tissue such as the breast; mesoscopy systems have also been applied clinically to visualise vascular network architectures in the skin given their limited penetration depths.[170]

Analysis

The acoustic wave generated in response to pulsed optical illumination depends on the absorption properties of tissue according to:

$$p_0(z) = \Gamma \mu_a F_0 e^{-\mu_0 z} \tag{13}$$

where p_0 is the initial pressure, Γ is the Gruneisen parameter, F_0 is the initial fluence, $\mu_0$is a constant, and z is the depth of the tissue.[171] Photoacoustic images are reconstructed using a range of beamforming methodologies, akin to ultrasound imaging.[163,171] 3D tomographic images can be reconstructed by combining the temporal and spatial information collected, often achieved analytically using a simple back-projection inversion or numerically using model-based methods.[171] Images reconstructed from data acquired at several wavelengths can then be subjected to the same multivariate analysis methods described in Section 4 for spectral

unmixing. However, frame-to-frame co-registration may be needed to avoid spatial or spectral corruption due to motion.

Limitations

The attainable depth of PAI depends on the optical and acoustic attenuation of the sample. In soft tissue, acoustic attenuation scales as a function of ultrasound frequency, so at low frequencies of a few MHz, optical attenuation tends to dominate and is the constraining factor for imaging depth.[171] For spatial resolution, the constraining factor is the bandwidth of the acoustic wave, usually limited by the acoustic attenuation of soft tissue and the frequency response of the detecting transducer.[172] The latter is particularly important for imaging more superficial features when the bandwidth of the signal can extend to 100 MHz and beyond, for which there is a limited availability of high-performance transducers. The maximum acoustic frequency transmitted decreases with depth, meaning that typically systems that operate at higher penetration depths have lower spatial resolutions than those designed for shallow imaging.[172]

A key challenge for PAI is biomarker quantification. During reconstruction, a number of assumptions are made, such as speed of sound in tissue, transducer impulse response, detection bandwidth, and continuous sampling.[171] If these assumptions break down, for example, due to heterogeneities in tissue due to air cavities, there will be distortions in the image. Furthermore, when evaluating biomarkers such as THb and sO_2, the nature of light propagation in tissue can lead to distortions in the spectral properties of the illumination as a function of depth. While some methods have been explored to compensate for such 'spectral coloring',[163,173] they often break down in the complex scenarios found in human tissue and have yet to be validated in a clinical setting. Finally, as with all hemoglobin sensing and

imaging methods, calibration of the extracted biomarkers is vital. PAI calibration and clinical quality assurance methods are still under development, particularly through a community-led effort.[174]

5.2 Diffuse Optical Spectroscopy and Imaging

Clinical research studies

Diffuse optical spectroscopy (DOS) is commonly referred to as near-infrared spectroscopy (NIRS) since it uses light in the near-infrared range; the term functional NIRS (fNIRS) is also commonly used but is usually restricted to applications monitoring functional responses to stimuli in the brain via neurovascular coupling. Quantifying and monitoring changes in oxygenation of blood in the brain has found many applications that range from understanding seizures[175] to detecting brain damage.[7] Unlike reflectance hemoglobin imaging (Fig. 6a-d), where an open cranium is required (see Section 4), fNIRS typically achieves imaging depths of up to 15 mm through the skull (Fig. 6e,f), which covers the outer cerebral cortex in healthy adults.[175–178] fNIRS imaging of the brain to identify intracranial hematomas due to brain trauma has been clinically approved by the FDA recently; however, it has yet to be widely deployed in clinical settings.[7]

Similar to PAI, DOI has also been deployed in clinical trials to detect cancer, particularly in the breast[179,180] (Fig. 5b,c) and thyroid,[177] where it has also been used to monitor response to therapy. DOI tends to be lower in spatial resolution than PAI (Fig. 5) but can often resolve other biomarkers in addition to hemoglobin. PAI typically has a lower temporal resolution compared to DOI.[181,182] In addition, DOI has been used to image muscle tissue such as the forearm, peripheral tissue, and joints.[177,178] Several reviews have been published illustrating the importance of DOI.[183–186]

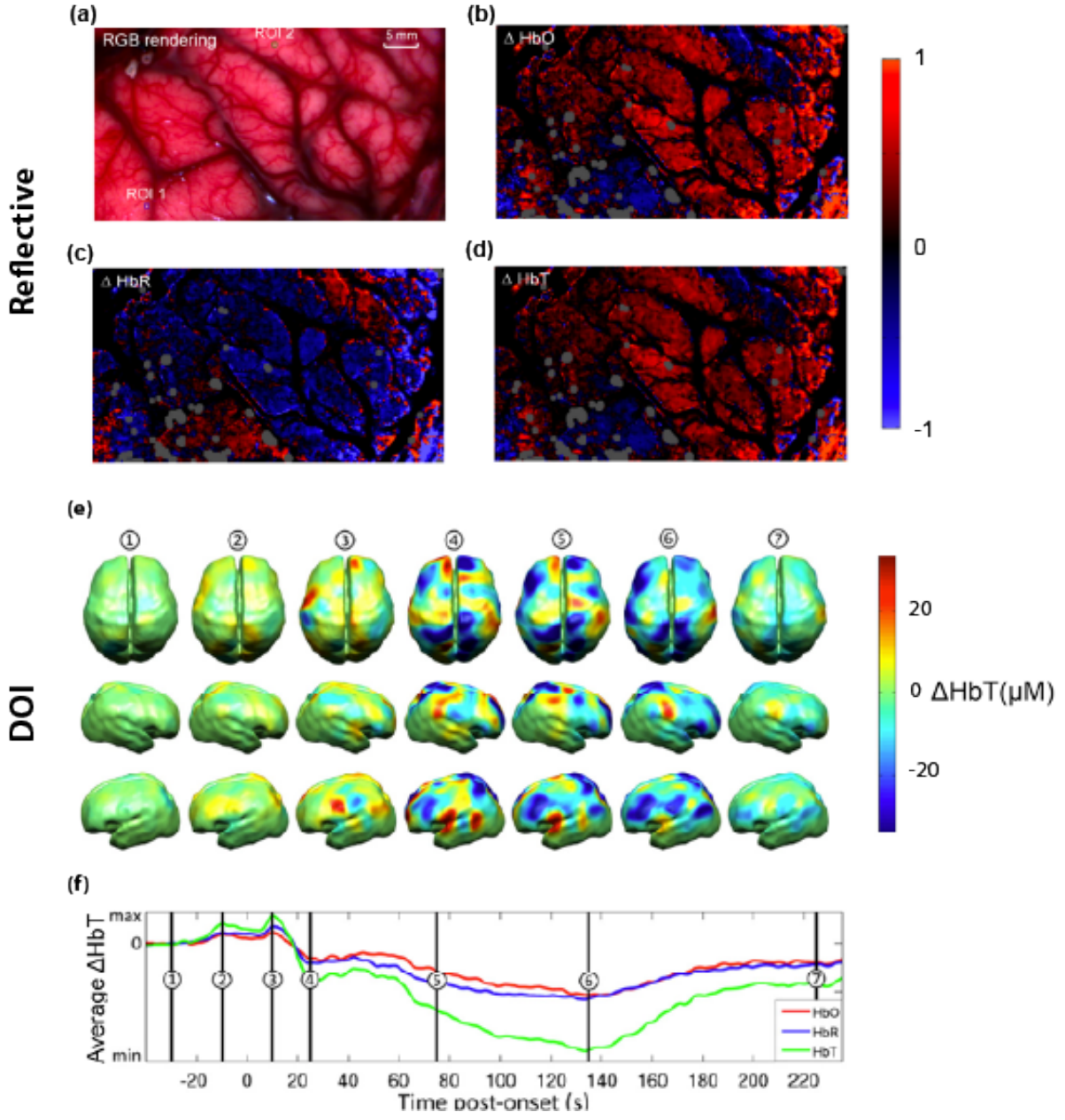

514

515 **Fig. 6: Hemoglobin imaging of the human brain**. (a-d) Reflectance spectral images of the
516 brain in an adult undergoing epileptogenic tissue resection: (a) Reference RGB rendering; (b)
517 Change in oxygenated hemoglobin over a single timeframe; (c) Change in deoxygenated
518 hemoglobin over a single timeframe; (d) Change in total hemoglobin over a single
519 timeframe.[108] (e-f) DOI of a neonate during a seizure: (e) changes in HbT concentration
520 mapped throughout the onset of a seizure; (f) average changes in Hb, HbO_2, and tHb post-onset
521 of the seizure.[175]

Technology

DOI techniques typically use near-infrared light in the 650 to 900 nm range.[177,178,181,183] Below 650 nm, light can experience poor penetration due to the absorption of hemoglobin in superficial tissues, while above 920 nm, water absorption comes to dominate.[178] Most DOI and fNIRS systems use two (or more) different wavelengths, one that is in the lower range below the NIR isosbestic point, such as 680, 695, 705, or 730 nm, and another that has a longer wavelength, such as 830 or 850 nm. The number of light sources and detectors varies depending on the system from 1 to more than 48, with some designed to allow for more light sources and detectors to enable customization of spatial resolution according to the target application.[181,187]

DOS is similar to DOI but provides single-point measurements of tissue properties such as hemoglobin and blood oxygen saturation similar to pulse oximetry.[188] There are three main modalities of DOS/I: continuous wave (CW), time-domain (TD), and frequency-domain (FD) systems.[177,178,181] CW systems detect changes in the intensity of illumination, making them relatively simple and inexpensive.[189] Slight changes in surface coupling can affect the intensity measurements, resulting in poor reproducibility unless well controlled. TD systems correlate the time between emission and detection of photons to measure the photon flight time. Tissue scattering determines photon flight time, while absorption determines the overall intensity of photons reaching the detector. FD systems are based on similar principles to time-domain systems but instead, measure the phase shift of the incoming light. Frequency domain systems are significantly less expensive than time-domain systems due to lower costs for the sensors and detectors. TD and FD systems can distinguish contaminating signals due to background illumination since these signals will be uncorrelated. Since TD and FD systems can separate out the effects of scattering and absorption these techniques can quantify absolute

concentrations of hemoglobin and its oxygenation, while CW systems typically measure the relative change in concentration, but not the absolute quantities.

DOI can be deployed in different geometries, either topographic, with imaging of a single plane with limited depth information, or tomographic (DOT), including depth resolution, which allows full 3D reconstruction of the pertinent properties of tissue. In transillumination techniques, the illumination and detection are on opposite sides of the tissue being imaged; however, this is limited to body parts with small radii. Measurements at multiple and overlapping source-detector separation can be used to create depth measurements and to reconstruct a 3D image. In tomographic systems, the illumination and detection sensors are placed on the available surface to simultaneously measure the changes in illumination throughout the sample.

Finally, it is worth noting that diffuse correlation spectroscopy (DCS) is similar to DOI and DOS but uses an autocorrelation function through a combination of hardware and software to measure an index of blood flow in tissue (Fig. 5c).[190] Due to the similarities in apparatus, sometimes DCS is combined with DOI or DOS systems[190] to provide a spatially-resolved indication of blood flow as a complementary biomarker to THb or sO_2.[190] Blood flow in tissue can also be detected using laser speckle contrast imaging (LCSI), which looks at fluctuations in the speckle pattern reflected from tissue to determine the flow rate of the blood.[191,192] Laser doppler flowmetry (LDF) finds the flow rate and concentration of blood by quantifying the Doppler shift that causes spectral broadening of reflected light. [192,193] All three of these techniques can resolve flow rate but they typically had relatively low spatial resolutions or are confined to single-point measurements. Recent advances, particularly in LCSI are now reaching near real-time operation at higher spatial resolutions, benefitting from increased computing power available in portable systems.[194]

Analysis

The analysis for DOI depends on the type of imaging system used. The measured signals can be converted into optical absorption maps by understanding the transport of light in tissue, which can be modeled using the radiative transport equation (RTE)[177,178] or Monte-Carlo methods. The RTE is an analytical approach, which approximates Maxwell's equations in diffuse media, assuming a constant refractive index. Solving the RTE is computationally expensive[178] but can be sped up by exploiting symmetries or by making approximations. For example, the diffusion approximation assumes isotropic scattering,[177] so it can be applied only in diffusive tissues; it does not work well in non-diffusive tissue, such as the cerebrospinal fluid that surrounds the brain or in anisotropic media, such as the skin and nervous system, where prior information is required to reach a solution. Numerical techniques, such as the finite element method, finite difference method, finite volume method, and boundary element method, can be used to solve the diffusion approximation. The use of prior information such as MRI, CT, or other imaging techniques can vastly improve DOI resolution by reducing the number of assumptions about the tissue structure that are made.[178]

Light transport can also be understood by forward modeling the propagation of light, using Monte-Carlo methods to calculate the propagation of photons through media. The accumulated forward modeling statistics can then be analyzed with respect to real data from DOI systems to address the inverse scattering problem for various anisotropic scattering media.[178] Monte-Carlo methods have traditionally also been computationally expensive but are now reaching higher speeds with deployment on GPU and cloud-based servers.[195]

Limitations

DOI exploits the scattering properties of tissue, unlike other imaging techniques that are hampered by light scattering. Despite this, DOI still has limited spatial resolution (on the order of 1 mm[183]) and often requires anatomical priors from another modality such as MRI or CT for analysis, which constrains applications[177,178,183,188] and adds cost and complexity to high-resolution DOI systems.[178] Standardization of DOI systems for clinical translation is ongoing, for example, through a project to characterize DOI systems using phantoms,[196] particularly for breast cancer detection.[197]

5.3 Spectroscopic OCT

Clinical research studies

While OCT is primarily deployed for structural imaging, its spectrally-resolved detection can be harnessed for angiography and oximetry *in vivo*, albeit not yet in clinical practice. OCT is typically implemented in the NIR for structural assessment due to its greater penetration through tissue and availability of light sources with suitable coherence. Extraction of blood sO_2 from OCT measurements in human retinal vasculature was first demonstrated in the NIR (800/850nm),[198] but had limited precision due to weak absorption in this range. The development of visible OCT systems improved the available signal-to-noise ratio and hence precision, enabling measurements from single erythrocytes[199,200] and high-resolution capillary oximetry in 3D.[201–203] Advances in reconstruction algorithms and high-speed instrumentation have improved OCT angiography to a point where it has found clinical use for high contrast imaging of retinal and dermal vasculature.[204,205] Visible OCT measurement of retinal sO_2 has been tested in humans[206] alongside angiography,[207] but is still in development. Laser exposure limits and natural aversion restrict the usable power level for visible OCT in the eye compared

to clinical NIR OCT, but continuing improvements in OCT technology have allowed high-quality imaging and sO_2 measurement.

Technology

OCT is a non-contact imaging modality that can be considered an optical analog of ultrasound imaging.[208] The distinguishing feature of OCT is the use of low-coherence interferometry to decouple the lateral and axial imaging resolution: lateral resolution is determined by the numerical aperture of the focusing optic, whereas axial resolution is determined by the temporal coherence of the laser used for imaging. Scanning OCT systems operate in the Fourier domain,[209] where a broad spectrum of light interrogates the tissue and is then collected through spectrally-resolved detection for post-processing and image reconstruction by an inverse Fourier transform. Within this class, there are two major varieties: Spectral Domain OCT (SD-OCT), which uses broadband illumination and parallel detection with a spectrometer, and Swept Source OCT (SS-OCT), which uses a high-speed spectral scanning source with single-channel detection for temporally-resolved spectral acquisition.

Recent advances in SS-OCT laser technology, including the tunable vertical-cavity source emitting laser, have enabled the realization of high-speed, robust, and compact instruments, which leads to greater imaging depths. Current SS-OCT systems operate exclusively in the NIR range due to swept laser availability; for imaging performance (and potential Hb oximetry) in the visible domain, SD-OCT systems using a visible spectrometer are required. In recent years, the high power and spatial coherence of newly available supercontinuum lasers have enabled good-quality visible OCT imaging in research systems,[210–212] which could enable future developments towards clinical translation.

Analysis

The raw data for SD-OCT is acquired from a high-speed spectrometer with line readout synchronized to a scanning mechanism, allowing for the mapping of each spectrum to a spatial position. The spectrum is normalized, filtered, and converted to a spatial reflectance profile, known as an A-line, through an inverse Fourier transform. For oximetry, the spectral domain of this analysis must be narrowed, typically through a windowing function; while full spectral resolution of the OCT volume may be realized through the application of the short-time Fourier transform, the dependence of axial resolution on spectral bandwidth poses a necessary trade-off between spectral resolution and axial resolution in the spectroscopic OCT image. For sO_2 measurement and spectral-contrast angiography, spectral windows are chosen to maximize the contrast of hemoglobin, typically in the range from 550-650 nm.[201,213] The spectrally-resolved total extinction coefficient is measured through depth fitting of the spectroscopic OCT A-line signal to the Beer-Lambert law, from which the relative contributions of Hb and HbO2 can be unmixed to determine sO_2.

Limitations

OCT is highly versatile, deployed for imaging the inner walls of blood vessels and luminal organs,[214–218] ultrawide field of view for scanning skin,[219–221] and with corrective lenses to compensate for ocular refraction in the ophthalmologic clinic. Nonetheless, there are several fundamental issues that are limiting general adoption. First, the scanned acquisition adds instrumental complexity and can produce motion artifacts in patients. While this is addressed in full-field OCT systems, these typically do not work with rough samples. Next, the spectral resolution of OCT imaging determines the maximum depth range that can be imaged; an aspect referred to as the sensitivity roll-off. Finally, because OCT is primarily sensitive to singly-scattered photons in tissue, the penetration depth of imaging is restricted to 1-2 mm in most human tissues. For this reason, large-scale clinical deployment of OCT has largely been limited

660 to ophthalmology, dermatology, and cardiology, but creative advances in OCT probe and
661 capsule technology will allow continued *in situ* exploration of hemoglobin-related biomarkers
662 from OCT in disease pathology throughout the body.[218,222–224]

Table 1: Overview of non-invasive hemoglobin monitoring and imaging

	Used to identify hypoxemia in a range of healthcare settings.	Single point measurement with no spatial resolution.	• Real-time monitoring of arterial saturation. • Extremely simple and quick to use in a clinical setting. • It can be used at the patient's bedside.	• Single point location measurement. • It can be inaccurate due to calibration assumptions • Errors are associated with variations in hemoglobin and poor perfusion on the tissue measured.	Commonly used in primary through to tertiary care. Potential for increased deployment at-home through wearables and low-cost devices.	13,48,70–72,51,54,57,62–65,69
	Diagnosing and monitoring systemic scleroderma and other arthritic conditions.	Spatial resolution varies from 0.1 to 10 μm laterally dependent upon the imaging NA, with corresponding imaging focal	• Real-time imaging of capillaries and blood flow is relatively easy. • Typically, the design is portable, so	• Lack of standardization around the quantification of capillary parameters. • Measures only structural, not functional,	Used in tertiary care. Emerging methods include quantification of blood flow, blood cell counts and oxygenation imaging.	5,100,225–234

		depth (Rayleigh range).	it can be used at the bedside if needed.	information about the capillaries. • Restricted to only imaging the nailfold capillaries.		
	Narrowband endoscopic imaging.	Spatial resolution varies from 5 to 400 μm depending on the application since most systems use lenses for magnification. Reflectance signal restricted to superficial ~200 μm of tissue due to scattering.	• A versatile method that can image multiple hemoglobin biomarkers as well as other proteins of interest • Relatively high spatial resolution is possible	• Processing of images can be complicated and is not always possible in real-time • Snapshot methods are fast but sacrifice spectral and spatial resolution • Scanning methods are slow but have a higher spectral resolution	Commonly used in tertiary care for endoscopic surveillance. Otherwise, in research and small-scale clinical trials with promising applications in cancer detection, skin lesions e.g. burns, and surgical tissue health.	2,6,113,117,118,235–240,8,46,84,87,98,105,106,108
	None at present.	PAM can have a spatial resolution of ~30 μm with an imaging depth	• Can assess the relative hemoglobin saturation together with other	• Trade-off between resolution and depth • Requires acoustic contact	Large scale clinical trials (n > 2000) for the diagnosis of breast cancer. Small scale clinical trials or proof of concept for other	28,141,164,171,172,174,241–246,142,247–251,143,153,158–161,163

		of around 2 to 6 mm PAT can have a resolution of ~200 μm with a penetration depth 2 to 3 cm.	biomarkers at depth while maintaining a reasonable spatial resolution. • It is a versatile technique scaling spatial resolution with depth of imaging required.	between the tissue and detectors. • Systems can be costly, though LEDs can be used at the expense of imaging quality. • The use of high power pulsed light can present additional safety considerations to ensure stray light does not damage patients and clinicians' eyes	applications, such as severity assessment in Crohn's disease and dermatological conditions.	
	Structural OCT is a clinical standard of care for retinal imaging. Spectroscopic OCT not yet clinically approved.	Lateral resolution determined by illumination optics, typically tens of μm but as low as 1-2 μm achievable. Axial resolution determined by	Real-time tomographic imaging with high resolution ideal for resolving tissue layers, structural characteristics in 3D.	• Optical scattering in tissue limits imaging depth to 1-2 mm for most tissues. • Laser scanning of sample introduces potential for motion artifacts	Structural OCT widely used in primary and tertiary centres for ophthalmology, dermatology, and dentistry, also in tertiary centres for cardiology. Spectroscopic OCT for oximetry in preclinical development.	[35,199–201,203,206–208,212,252–256]

		source/detector bandwidth, on order of tens of μm down to 1 μm. Penetration depth limited to ~1 mm in medium-scattering tissue.		in image, ophthalmic visible OCT implementation limited by safety threshold and patient aversion.		
	Assessment of brain activity (fNIRS or DOT). Monitoring of tissue oxygenation (cerebral oximetry/NIRS).	1 to 30 mm spatial resolution; high resolutions are only possible at shallow imaging depths (<2cm). Low-resolution imaging is possible up to 10 cm into the tissue.	Capable of determining blood oxygenation in tissue and other chromophores such as melanin, lipids, cytochrome-c-oxidase, and water.	• Relatively low resolution; to obtain high-resolution requires prior knowledge of tissue composition and a high density of optodes. • DOI techniques may be combined with other imaging modalities such as MRI or ultrasound to assess tissue composition,	Clinical approval and small-scale clinical use of tissue oximetry/NIRS for assessment of brain oxygenation. fNIRS/DOT used commonly as research tool to monitor brain activity. Small scale clinical trials or proof of concept for other applications, such as breast cancer diagnosis, joint inflammation.	[124,144,261,262,145,146,177,190,257–260]

[redacted]				resulting in increased system cost. • Computationally intensive and time-consuming, resulting in limited real-time imaging (spectroscopy does not have this problem).		

664

6: Summary and Perspective

Moving beyond pulse oximetry to exploit the optical absorption of hemoglobin in imaging applications has shown significant promise in the clinic, with both superficial 2D and depth-resolved 3D implementations described in this review. Two wavelength THb and sO_2 imaging are already widely used in endoscopic and ophthalmic applications, respectively, and have reached large-scale clinical trials in depth-resolved photoacoustic imaging. Conversely, reflectance-based spectral imaging remains largely exploratory.

Trade offs

Choosing the optimal hemoglobin imaging technique for a particular application involves consideration of several factors that often require trade-offs, including: signal-to-noise ratio; spatial and temporal resolution; target depth; and route to integration with existing clinical practice. Optical imaging techniques are ultimately restricted by the maximum permissible exposure at the illumination site, which places a fundamental limit on the signal-to-noise ratio available in the clinical setting. Some techniques are further restricted in the type of illumination used, such as OCT that requires coherent light, or PAI that requires short, pulsed light, which can add to the complexity of safety considerations in the clinic.

Considering the factors of resolution and depth, reflectance-based imaging can achieve high spatiotemporal resolution in applications where depth-resolution is not vital, for example, with retinal, endoscopic or intraoperative imaging. One could argue depth-resolution will become increasingly prevalent with the emergence of more advanced solutions from spectroscopic OCT, PAI and DOI, particularly as costs reduce. Nonetheless, depth-resolution typically implies a sacrifice of spatial or temporal resolution, which must be determined early in the discovery and development phase of the associated device. Furthermore, different

approaches to achieving depth resolution have different strengths and weaknesses. PAI may suffer from shielding effects due to the absorption of overlying tissue and tends to resolve only larger vessels, while the use of multiple scattering by DOI enables better detection of capillary oxygenation, despite the overall poorer spatial resolution. This trade-off may explain why PAI has developed more rapidly in clinical translation for breast cancer detection, while DOI is more developed for imaging the brain. Given the common contrast source across many of the techniques described, it may also be desirable to combine multiple approaches in a single device for validation purposes or to provide views of the same tissue at different resolution scales, overcoming some of the limitations of the existing technologies.[263] Combining two or more optical imaging techniques can be beneficial since they reduce the imaging limitations that arise as a result of a single technique. A good example of this is the enhanced perfusion oximetry system (EPOS) that combines Diffuse Reflectance Spectroscopy with Laser Doppler Flowmetry to quantify blood oxygenation and flow rate for imaging of microvasculature and burns.[264–266]

Clinical implementation

There are many factors to consider regarding the route to integration of new techniques into clinical practice. For example, if imaging is required to be non-contact, for example in delicate targets like the eye, this may restrict the implementation of methods such as PAI or DOI, where contact with the tissue is typically required. The pathway to clinical adoption may be smoother in the case where an existing optical imaging solution is already deployed. An obvious example is the large-scale deployment of OCT for ophthalmic applications, which provides a direct route for adoption of spectroscopic OCT in the community. Another factor in clinical translation is the assessment of the precision, accuracy and bias of new biomarker measurements.[2] These factors can be affected by both device operation and data interpretation,

requiring standardisation of data acquisition and careful consideration of any signal processing or analysis methods applied before presenting the data to the interpreter, whether this is a human or a machine. Since reflectance-based imaging techniques are usually less computationally intensive compared to the depth-resolved methods, the development of systems and software for real-time imaging is more easily attainable; this is seen most effectively in narrowband imaging of blood vessels in endoscopy.

Further clinical considerations arise later in the translational pathway when the question of biomarker efficacy in decision-making finally arises. Instrument prototypes are often used first in pilot clinical trials at a single clinical center to gather initial data for validation and may be subject to multiple design iterations at this stage. Having successfully passed the first translational gap, which may include CE marking or FDA approval for the device and multi-center clinical trials, the technique is then subject to advanced qualification and ongoing technical validation to determine clinical utility in the healthcare setting, whereby the measurement can be used in clinical decision making. These larger-scale clinical trials help to determine sources of variation that will influence the classification and diagnosis of disease, providing clinical evidence of the ability to change patient management. They also provide extensive reference data sets that can be used to improve interpretation, particularly where machine learning-based methods are involved.

Reflectance based spectral imaging techniques are still largely in the earlier stages of development with first in-person trials, while fNIRS of the brain and PAI of the breast is being used in multiple centers as part of larger-scale clinical trials and DOI has found some level of adoption into the clinic.[84,142,150,181,184,267] Data arising from these trials is extremely valuable and making annotated datasets open-source for the community will not only help accelerate

735 the development of new algorithms but could also enhance our understanding of the biology
736 of hemoglobin oxygenation in disease.

737 *Disease monitoring*

738 Hemoglobin imaging methods could find further applications in monitoring disease, to
739 detect treatment efficacy or disease relapse. The non-invasive nature of these techniques can
740 allow continuous or periodic monitoring, for which there are several excellent examples that
741 have been highlighted. Pulse oximetry can be applied to a patient for long periods so that
742 clinicians can observe if there are any changes to overall arterial oxygenation. DOI and NIRS
743 also can be used longitudinally to monitor changes in brain function to assess if there is
744 improved brain activity.[267] Furthermore, periodic monitoring of diseases such as scleroderma
745 using nailfold capillaroscopy can indicate progression in the stage and severity of the disease,
746 which may influence the treatment provided or indicate further medical intervention is
747 required.

748 Periodic monitoring can be applied in the short term, for monitoring wound or burn
749 healing, or in the longer term in the context of endoscopic cancer surveillance in at-risk patient
750 groups such as those with Barrett's oesophagus that are at increased risk of developing cancer.
751 The frequency of monitoring applied is determined by the disease being observed and the rate
752 at which change is expected, as well as by the training required for instrument use and data
753 interpretation. For example, applying pulse oximetry is relatively quick; non-specialists can do
754 it, and some more straightforward versions of capillaroscopy can be done using handheld
755 devices. Conversely, endoscopies, OCT, DOI, and NIRS typically require training of specialist
756 operators hence it can be more expensive to conduct the procedures, meaning they are typically
757 be used for less frequent monitoring.

Outlook

The acceptability and relevance of new hemoglobin sensing and imaging technologies to clinicians will be driven by various factors, including cost, complexity, and physical size of the systems, as well as ease of use and data interpretation. The commonplace use of pulse oximetry means that the clinical community is already well aware of the use of systemic sO_2 as a disease biomarker. Ongoing technological developments that lead to miniaturization of light sources, optical components, and cameras, as well as decreasing their cost, mitigate some of the technical limitations highlighted in this review. Advances in image processing including convolutional neural networks promise to aid in distilling rich datasets to actionable clinical information, enabling imaging systems to be more easily integrated into clinical care. Research questions remain regarding the sensitivity of hemoglobin sensing techniques in diverse populations and the diagnostic power of hemoglobin-derived biomarkers in the wide array of disease presentations included in this review that will only be answered through comprehensive clinical trials. Hemoglobin imaging techniques add a new dimension of knowledge in a range of clinical settings, from capillaroscopy and endoscopy to intraoperative imaging; emerging technologies are well placed to further enhance these areas of existing clinical practice, but are also likely to contribute to the decentralization of healthcare to tertiary care centers and through the deployment of wearable technologies for self-monitoring in the home.

Acknowledgments: Grant Support: M. T-W. acknowledges the financial support of the General Sir John Monash Foundation and the Cambridge Trust. GB is supported by the Gianna Angelopoulos Programme for Science Technology and Innovation. GS and SEB funding from the EPSRC (EP/R003599/1) and CRUK (C9545/A29580).

781 **Disclosure:** The authors have no conflicts of interest to declare.

782

References

1. J. P. B. B. O'Connor et al., "Imaging biomarker roadmap for cancer studies," Nat. Rev. Clin. Oncol. **14**(3), 169–186, Nature Publishing Group (2017) [doi:10.1038/nrclinonc.2016.162].

2. D. J. Waterhouse et al., "A roadmap for the clinical implementation of optical-imaging biomarkers," Nat. Biomed. Eng. **3**(5), 339–353 (2019) [doi:10.1038/s41551-019-0392-5].

3. J. Levy et al., "Digital oximetry biomarkers for assessing respiratory function: standards of measurement, physiological interpretation, and clinical use," npj Digit. Med. **4**(1), Springer US (2021) [doi:10.1038/s41746-020-00373-5].

4. A. S. Scott, M. A. Baltzan, and N. Wolkove, "Examination of pulse oximetry tracings to detect obstructive sleep apnea in patients with advanced chronic obstructive pulmonary disease," Can. Respir. J. **21**(3), 171–175 (2014) [doi:10.1155/2014/948717].

5. G. Dinsdale et al., "State-of-the-art technologies provide new insights linking skin and blood vessel abnormalities in SSc-related disorders," Microvasc. Res. **130**(April), 104006, Elsevier (2020) [doi:10.1016/j.mvr.2020.104006].

6. A. Nouvong et al., "Evaluation of diabetic foot ulcer healing with hyperspectral imaging of oxyhemoglobin and deoxyhemoglobin," Diabetes Care **32**(11), 2056–2061 (2009) [doi:10.2337/dc08-2246].

7. C. S. Robertson et al., "Clinical evaluation of a portable near-infrared device for

detection of traumatic intracranial hematomas," J. Neurotrauma **27**(9), 1597–1604 (2010) [doi:10.1089/neu.2010.1340].

8. M. S. Chin et al., "Hyperspectral imaging for burn depth assessment in an animal model," Plast. Reconstr. Surg. - Glob. Open **3**(12), 1–9 (2015) [doi:10.1097/GOX.0000000000000558].

9. A. Roggan et al., "Optical properties of circulating human blood in the wavelength range 400-2500 nm," J. Biomed. Opt. **4(1)**(January 1999), 36–46 (1999).

10. M. L. Turgeon, *Clinical Hematology : Theory and Procedures*, 2nd ed., Little, Brown, Boston ; London (1993).

11. I. J. Bigio and S. Fantini, "Overview of tissue optical properties," in Quantitative Biomedical Optics: Theory, Methods, and Applications, 1st ed., pp. 19–59, Cambridge University Press (2016) [doi:10.1017/CBO9781139029797].

12. T. Vos et al., "Global, regional, and national incidence, prevalence, and years lived with disability for 310 diseases and injuries, 1990–2015: A systematic analysis for the Global Burden of Disease Study 2015," Lancet **388**(10053), 1545–1602 (2016) [doi:10.1016/S0140-6736(16)31678-6].

13. M. Nitzan, A. Romem, and R. Koppel, "Pulse oximetry: Fundamentals and technology update," Med. Devices Evid. Res. **7**(1), 231–239 (2014) [doi:10.2147/MDER.S47319].

14. W. Shin, Y. D. Cha, and G. Yoon, "ECG/PPG integer signal processing for a ubiquitous health monitoring system," J. Med. Syst. **34**(5), 891–898 (2010) [doi:10.1007/s10916-009-9304-7].

15. B. A. Darlow and C. J. Morley, “Oxygen Saturation Targeting and Bronchopulmonary Dysplasia,” Clin. Perinatol. **42**(4), 807–823 (2015) [doi:10.1016/j.clp.2015.08.008].

16. N. W. Tietz and E. A. Fiereck, “The Spectrophotometric Measurement of Carboxyhemoglobin,” Ann. Clin. Lab. Sci. **3**(1) (1973).

17. L. Gharahbaghian, B. Massoudian, and G. Dimassa, “Methemoglobinemia and sulfhemoglobinemia in two pediatric patients after ingestion of hydroxylamine sulfate.,” West. J. Emerg. Med. **10**(3), 197–201 (2009).

18. E. Dervieux, Q. Bodinier, and W. Uhring, “Measuring hemoglobin spectra : searching for carbamino-hemoglobin” (2020) [doi:10.1117/1.JBO.25.10.105001].

19. M. Van Gastel, S. Stuijk, and G. De Haan, “Camera-based pulse-oximetry - validated risks and opportunities from theoretical analysis,” Biomed. Opt. Express **9**(1), 102 (2018) [doi:10.1364/boe.9.000102].

20. J. K. Barton et al., “Cooperative Phenomena in Two-pulse, Two-color Laser Photocoagulation of Cutaneous Blood Vessels¶,” Photochem. Photobiol. **73**(6), 642 (2001) [doi:10.1562/0031-8655(2001)073<0642:cpitpt>2.0.co;2].

21. L. L. Randeberg et al., “Methemoglobin formation during laser induced photothermolysis of vascular skin lesions,” Lasers Surg. Med. **34**(5), 414–419 (2004) [doi:10.1002/lsm.20042].

22. S. R. David et al., “The blood blues: A review on methemoglobinemia,” J. Pharmacol. Pharmacother. **9**(1), 1–5 (2018) [doi:10.4103/jpp.JPP_79_17].

23. C. S. Thom et al., “Hemoglobin variants: Biochemical properties and clinical

correlates," Cold Spring Harb. Perspect. Med. **3**(3) (2013) [doi:10.1101/cshperspect.a011858].

24. L. Tofani et al., "Spectroscopic and interfacial properties of myoglobin/surfactant complexes," Biophys. J. **87**(2), 1186–1195 (2004) [doi:10.1529/biophysj.104.041731].

25. L. S. L. Arakaki, D. H. Burns, and M. J. Kushmerick, "Accurate myoglobin oxygen saturation by optical spectroscopy measured in blood-perfused rat muscle," Appl. Spectrosc. **61**(9), 978–985 (2007) [doi:10.1366/000370207781745928].

26. G. Lu and B. Fei, "Medical hyperspectral imaging: a review," J. Biomed. Opt. **19**(1), 010901 (2014) [doi:10.1117/1.jbo.19.1.010901].

27. V. V. V. V. V Tuchin, *Tissue Optics: Light Scattering Methods and Instruments for Medical Diagnosis*, Third Edit, in SPIE Pres, Third Edit, Bellingham, Washington, USA (2015) [doi:10.1117/3.684093].

28. J. Yao and L. V. Wang, "Sensitivity of photoacoustic microscopy," Photoacoustics **2**(2), 87–101, Elsevier GmbH. (2014) [doi:10.1016/j.pacs.2014.04.002].

29. W. G. Zijlstra, A. Buursma, and W. P. Meeuwsen-van der Roest, "Absorption spectra of human fetal and adult oxyhemoglobin, de-oxyhemoglobin, carboxyhemoglobin, and methemoglobin," Clin. Chem. **37**(9), 1633–1638 (1991).

30. A. P. Harris et al., "Absorption characteristics of human fetal hemoglobin at wavelengths used in pulse oximetry," J. Clin. Monit. **4**(3), 175–177 (1988) [doi:10.1007/BF01621812].

31. K. A. Shapovalov, "The geometry and optical models of the erythrocyte," Syst. Rev.

Pharm. **11**(12), 1456–1463 (2020) [doi:10.31838/srp.2020.12.216].

32. M. Kinnunen et al., "Effect of the size and shape of a red blood cell on elastic light scattering properties at the single-cell level," Biomed. Opt. Express **2**(7), 1803 (2011) [doi:10.1364/boe.2.001803].

33. J. Gienger et al., "Refractive index of human red blood cells between 290 nm and 1100 nm determined by optical extinction measurements," Sci. Rep. **9**(1), 1–11 (2019) [doi:10.1038/s41598-019-38767-5].

34. D. J. Faber, F. J. Van Der Meer, and M. C. G. Aalders, "Quantitative measurement of attenuation coefficients of weakly scattering media using optical coherence tomography," Opt. Express **12**(19), 590–592 (2004).

35. R. Liu et al., "Theoretical model for optical oximetry at the capillary level: exploring hemoglobin oxygen saturation through backscattering of single red blood cells," J. Biomed. Opt. **22**(2), 025002 (2017) [doi:10.1117/1.jbo.22.2.025002].

36. R. Liu et al., "Single capillary oximetry and tissue ultrastructural sensing by dual-band dual-scan inverse spectroscopic optical coherence tomography," Light Sci. Appl. **7**(1), 57 (2018) [doi:10.1038/s41377-018-0057-2].

37. N. Bosschaart et al., "A literature review and novel theoretical approach on the optical properties of whole blood," Lasers Med. Sci. **29**(2), 453–479 (2014) [doi:10.1007/s10103-013-1446-7].

38. M. Meinke et al., "Optical properties of platelets and blood plasma and their influence on the optical behavior of whole blood in the visible to near infrared wavelength

range," J. Biomed. Opt. **12**(1), 014024 (2007) [doi:10.1117/1.2435177].

39. M. Meinke et al., "Empirical model functions to calculate hematocrit-dependent optical properties of human blood," Appl. Opt. **46**(10), 1742–1753 (2007) [doi:10.1364/AO.46.001742].

40. M. Friebel et al., "Influence of oxygen saturation on the optical scattering properties of human red blood cells in the spectral range 250 to 2000 nm," J. Biomed. Opt. **14**(3), 034001 (2009) [doi:10.1117/1.3127200].

41. T. Saito and H. Yamaguchi, "Optical imaging of hemoglobin oxygen saturation using a small number of spectral images for endoscopic imaging," J. Biomed. Opt. **20(12)**(126011), 126011 (2015) [doi:10.1117/1.JBO.20.12.126011].

42. S. L. Jacques, "Optical properties of biological tissues: A review," Phys. Med. Biol. **58**(11), R37-61 (2013) [doi:10.1088/0031-9155/58/11/R37].

43. A. J. Welch, M. J. C. van Gemert, and J. T. Walsh, "Basic Interactions of Light with Tissue," in Optical-Thermal Response of Laser-Irradiated Tissue, pp. 13–26, Springer Netherlands :, Dordrecht : (2011) [doi:10.1007/978-90-481-8831-4_2].

44. S. A. Prahl, "Tabulated Molar Extinction Coefficient for Hemoglobin in Water," 1998, <http://omlc.ogi.edu/spectra/hemoglobin/summary.html>.

45. O. Siggaard-Andersen, B. Nørgaard-Pedersen, and J. Rem, "Hemoglobin pigments. spectrophotometric determination of oxy-, carboxy-, met-, and sulfhemoglobin in capillary blood," Clin. Chim. Acta **42**(1), 85–100 (1972) [doi:10.1016/0009-8981(72)90380-4].

909 46. L. L. Randeberg and J. Hernandez-Palacios, “Hyperspectral imaging of bruises in the
910 SWIR spectral region,” Photonic Ther. Diagnostics VIII **8207**(February 2012),
911 82070N (2012) [doi:10.1117/12.909137].

912 47. I. H. Yarynovska and A. I. Bilyi, “Absorption spectra of sulfhemoglobin derivates of
913 human blood,” Opt. Diagnostics Sens. VI **6094**(February 2006), 60940G (2006)
914 [doi:10.1117/12.639597].

915 48. A. Reisner et al., “Utility of the photoplethysmogram in circulatory monitoring,”
916 Anesthesiology **108**(5), 950–958 (2008) [doi:10.1097/ALN.0b013e31816c89e1].

917 49. P. D. Mannheimer, “The light-tissue interaction of pulse oximetry,” Anesth. Analg.
918 **105**(SUPPL. 6) (2007) [doi:10.1213/01.ane.0000269522.84942.54].

919 50. J. T. B. Moyle, “Uses and abuses of pulse oximetry,” Arch. Dis. Child. **74**(1), 77–80
920 (1996) [doi:10.1136/adc.74.1.77].

921 51. J. E. Sinex, “Pulse oximetry: Principles and limitations,” Am. J. Emerg. Med. **17**(1),
922 59–66 (1999) [doi:10.1016/S0735-6757(99)90019-0].

923 52. A. M. Luks and E. R. Swenson, “Pulse oximetry for monitoring patients with COVID-
924 19 at home potential pitfalls and practical guidance,” Ann. Am. Thorac. Soc. **17**(9),
925 1040–1046 (2020) [doi:10.1513/AnnalsATS.202005-418FR].

926 53. A. Jubran, “Pulse oximetry,” Intensive Care Med. **31**(11), 1598 (2005)
927 [doi:10.1007/s00134-005-2798-7].

928 54. G. Tusman, S. H. Bohm, and F. Suarez-Sipmann, “Advanced Uses of Pulse Oximetry
929 for Monitoring Mechanically Ventilated Patients,” Anesth. Analg. **124**(1), 62–71

(2017) [doi:10.1213/ANE.0000000000001283].

55. M. Kluckow, “Barriers to the implementation of newborn pulse oximetry screening: A different perspective,” Int. J. Neonatal Screen. **4**(1) (2018) [doi:10.3390/ijns4010004].

56. Z. Mosayebi et al., “Evaluation of pulse oximetry in the early diagnosis of cardiac and noncardiac diseases in healthy newborns,” Iran. J. Neonatol. **11**(1), 43–50 (2020) [doi:10.22038/ijn.2019.38511.1608].

57. H. Lee et al., “Toward all-day wearable health monitoring: An ultralow-power, reflective organic pulse oximetry sensing patch,” Sci. Adv. **4**(11), 1–9 (2018) [doi:10.1126/sciadv.aas9530].

58. A. Fawzy et al., “Racial and Ethnic Discrepancy in Pulse Oximetry and Delayed Identification of Treatment Eligibility Among Patients With COVID-19,” 1–9 (2022) [doi:10.1001/jamainternmed.2022.1906].

59. M. W. Sjoding et al., “Racial Bias in Pulse Oximetry Measurement,” N. Engl. J. Med. **383**(25), 2477–2478 (2020) [doi:10.1056/nejmc2029240].

60. A. Jubran, “Pulse oximetry,” Intensive Care Med. **19**(1), 1–7, Critical Care (2005) [doi:10.1186/s13054-015-0984-8].

61. E. D. Chan, M. M. Chan, and M. M. Chan, “Pulse oximetry: Understanding its basic principles facilitates appreciation of its limitations,” Respir. Med. **107**(6), 789–799, Elsevier Ltd (2013) [doi:10.1016/j.rmed.2013.02.004].

62. S. Lopez, “Pulse Oximeter Fundamentals and Design,” Free. Semicond. Inc., 1–39 (2012).

63. O. Y. Hay et al., “Pulse oximetry with two infrared wavelengths without calibration in extracted arterial blood,” Sensors (Switzerland) **18**(10) (2018) [doi:10.3390/s18103457].

64. M. P. McEwen, G. P. Bull, and K. J. Reynolds, “Vessel calibre and haemoglobin effects on pulse oximetry,” Physiol. Meas. **30**(9), 869–883 (2009) [doi:10.1088/0967-3334/30/9/001].

65. E. Hill and M. D. Stoneham, “Practical applications of pulse oximetry,” Updat. Anaesth. **5**(11), 11–15 (2000).

66. J. Nixdorff et al., “Comparison of Transmittance and Reflectance Pulse Oximetry in Anesthetized Dogs,” Front. Vet. Sci. **8**(April), 1–7 (2021) [doi:10.3389/fvets.2021.643966].

67. R. W. C. G. R. Wijshoff et al., “Reducing motion artifacts in photoplethysmograms by using relative sensor motion: phantom study,” J. Biomed. Opt. **17**(11), 117007 (2012) [doi:10.1117/1 .JBO.17.11.117007].

68. H. Zhang et al., “Wireless, battery-free optoelectronic systems as subdermal implants for local tissue oximetry,” Sci. Adv. **5**(3) (2019) [doi:10.1126/sciadv.aaw0873].

69. T. Y. Abay and P. A. Kyriacou, “Comparison of NIRS, laser Doppler flowmetry, photoplethysmography, and pulse oximetry during vascular occlusion challenges,” Physiol. Meas. **37**(4), 503–514, IOP Publishing (2016) [doi:10.1088/0967-3334/37/4/503].

70. C. Liu et al., “Optical fibre-based pulse oximetry sensor with contact force detection,”

Sensors (Switzerland) **18**(11) (2018) [doi:10.3390/s18113632].

71. W. Verkruysse et al., "Calibration of Contactless Pulse Oximetry," Anesth. Analg. **124**(1), 136–145 (2017) [doi:10.1213/ANE.0000000000001381].

72. J. Kim et al., "Miniaturized Battery-Free Wireless Systems for Wearable Pulse Oximetry," Adv. Funct. Mater. **27**(1), 1–8 (2017) [doi:10.1002/adfm.201604373].

73. L. E. Mackenzie and A. R. Harvey, "Oximetry using multispectral imaging: Theory and application," J. Opt. (United Kingdom) **20**(6), IOP Publishing (2018) [doi:10.1088/2040-8986/aab74c].

74. M. Nitzan and S. Engelberg, "Three-wavelength technique for the measurement of oxygen saturation in arterial blood and in venous blood," J. Biomed. Opt. **14**(2), 024046 (2009) [doi:10.1117/1.3120496].

75. Q. J. W. Milner and G. R. Mathews, "An assessment of the accuracy of pulse oximeters," Anaesthesia **67**(4), 396–401 (2012) [doi:10.1111/j.1365-2044.2011.07021.x].

76. M. Oura et al., "Calibration system for pulse spectrophotometry using a double-layer pulsation flow-cell," Proc. 31st Annu. Int. Conf. IEEE Eng. Med. Biol. Soc. Eng. Futur. Biomed. EMBC 2009, 896–899, IEEE (2009) [doi:10.1109/IEMBS.2009.5334889].

77. V. N. D. Le et al., "Calibration of Spectral Imaging Devices With Oxygenation-Controlled Phantoms: Introducing a Simple Gel-Based Hemoglobin Model," Front. Phys. **7**(November), 1–7 (2019) [doi:10.3389/fphy.2019.00192].

78. J. E. Yount, “Devices and Procedures for In Vitro Testing of Pulse Oximetry Monitors,” 4,968,137, p. US Patent: 4,968,137, United States (1990).

79. S. J. Barker and K. K. Tremper, “The effect of carbon monoxide inhalation on pulse oximetry and transcutaneous PO2,” Anesthesiology **66**(5), 677–679 (1987).

80. C. D. Corporation, “SmartSat Benchtop,” Journal of Clinical Monitoring and Computing **17**(3–4), 2002, [doi:10.1023/A:1020795307742].

81. M. Nitzan et al., “Calibration-free pulse oximetry based on two wavelengths in the infrared - A preliminary study,” Sensors (Switzerland) **14**(4), 7420–7434 (2014) [doi:10.3390/s140407420].

82. S. J. Barker et al., “Measurement of carboxyhemoglobin and methemoglobin by pulse oximetry: A human volunteer study,” Anesthesiology **105**(5), 892–897 (2006) [doi:10.1097/00000542-200611000-00008].

83. P. E. Bickler, J. R. Feiner, and J. W. Severinghaus, “Effects of skin pigmentation on pulse oximeter accuracy at low saturation,” Anesthesiology **102**(4), 715–719 (2005) [doi:10.1097/00000542-200504000-00004].

84. N. T. Clancy et al., “Surgical spectral imaging,” Med. Image Anal. **63**, 101699, Elsevier B.V. (2020) [doi:10.1016/j.media.2020.101699].

85. Q. Li et al., “Review of spectral imaging technology in biomedical engineering: achievements and challenges,” J. Biomed. Opt. **18**(10), 100901 (2013) [doi:10.1117/1.jbo.18.10.100901].

86. H. L. H. L. Offerhaus, S. E. S. E. S. E. Bohndiek, and A. R. A. R. Harvey,

"Hyperspectral imaging in biomedical applications," J. Opt. (United Kingdom) **21**(1), IOP Publishing (2019) [doi:10.1088/2040-8986/aaf2a0].

87. J. Yoon et al., "A clinically translatable hyperspectral endoscopy (HySE) system for imaging the gastrointestinal tract," Nat. Commun. **10**(1), 1–13, Springer US (2019) [doi:10.1038/s41467-019-09484-4].

88. E. Häggblad et al., "Reflection spectroscopy of analgesized skin," Microvasc. Res. **62**(3), 392–400 (2001) [doi:10.1006/mvre.2001.2358].

89. L. Giannoni, F. Lange, and I. Tachtsidis, "Hyperspectral imaging solutions for brain tissue metabolic and hemodynamic monitoring: Past, current and future developments," J. Opt. (United Kingdom) **20**(4), 44009, IOP Publishing (2018) [doi:10.1088/2040-8986/aab3a6].

90. T. W. Sawyer et al., "Opti-MSFA: a toolbox for generalized design and optimization of multispectral filter arrays," Opt. Express **30**(5), 7591 (2022) [doi:10.1364/oe.446767].

91. M. Taylor-Williams et al., "Spectrally tailored 'hyperpixel' filter arrays for imaging of chemical compositions," Proc. SPIE BiOS **11954**(March), 23 (2022) [doi:10.1117/12.2606917].

92. P. Lukes et al., "Narrow Band Imaging (NBI) — Endoscopic Method for Detection of Head and Neck Cancer," Endoscopy (2013) [doi:10.5772/52738].

93. Q. Li et al., "Estimation of tissue oxygen saturation from RGB images and sparse hyperspectral signals based on conditional generative adversarial network," Int. J.

Comput. Assist. Radiol. Surg. **14**(6), 987–995, Springer International Publishing (2019) [doi:10.1007/s11548-019-01940-2].

94. D. S. Terman et al., "Sickle Erythrocytes Target Cytotoxics to Hypoxic Tumor Microvessels and Potentiate a Tumoricidal Response," PLoS One **8**(1), 1–11 (2013) [doi:10.1371/journal.pone.0052543].

95. S. Beg, A. Wilson, and K. Ragunath, "The use of optical imaging techniques in the gastrointestinal tract," Frontline Gastroenterol. **7**(3), 207–215 (2016) [doi:10.1136/flgastro-2015-100563].

96. S. J. Spechler et al., "American gastroenterological association technical review on the management of Barrett's esophagus," Gastroenterology **140**(3), 18–52 (2011) [doi:10.1053/j.gastro.2011.01.031].

97. J. Yoon et al., "First experience in clinical application of hyperspectral endoscopy for evaluation of colonic polyps," J. Biophotonics(March), 1–9 (2021) [doi:10.1002/jbio.202100078].

98. A. S. Luthman et al., "Bimodal reflectance and fluorescence multispectral endoscopy based on spectrally resolving detector arrays," J. Biomed. Opt. **24**(03), 1 (2018) [doi:10.1117/1.jbo.24.3.031009].

99. D. J. Waterhouse et al., "Spectral endoscopy enhances contrast for neoplasia in surveillance of Barrett's esophagus," Cancer Res. **81**(12), 3415–3425 (2021) [doi:10.1158/0008-5472.CAN-21-0474].

100. S. N. Lambova and U. Müller-Ladner, "Nailfold capillaroscopy in systemic sclerosis –

state of the art: The evolving knowledge about capillaroscopic abnormalities in systemic sclerosis," J. Scleroderma Relat. Disord. **4**(3), 200–211 (2019) [doi:10.1177/2397198319833486].

101. V. Dremin et al., "Dynamic evaluation of blood flow microcirculation by combined use of the laser Doppler flowmetry and high-speed videocapillaroscopy methods," J. Biophotonics **12**(6), 1–7 (2019) [doi:10.1002/jbio.201800317].

102. M. V. Volkov et al., "Evaluation of blood microcirculation parameters by combined use of laser Doppler flowmetry and videocapillaroscopy methods," Saratov Fall Meet. 2016 Opt. Technol. Biophys. Med. XVIII **10336**(November), 1033607 (2017) [doi:10.1117/12.2267955].

103. U. Baran, L. Shi, and R. K. Wang, "Capillary blood flow imaging within human finger cuticle using optical microangiography," J. Biophotonics **8**(0), 46–51 (2015) [doi:10.1038/jid.2014.371].

104. W. F. Yip et al., "Reliability and determinants of retinal vessel oximetry measurements in healthy eyes," Investig. Ophthalmol. Vis. Sci. **55**(11), 7104–7110 (2014) [doi:10.1167/iovs.13-13854].

105. R. Podlipec et al., "Characterization of blood coagulation dynamics and oxygenation in ex-vivo retinal vessels by fluorescence hyperspectral imaging," J. Biophotonics(April), 1–12 (2020) [doi:10.1002/jbio.202000021].

106. X. Hadoux et al., "Non-invasive in vivo hyperspectral imaging of the retina for potential biomarker use in Alzheimer's disease," Nat. Commun. **10**(1), 1–12 (2019) [doi:10.1038/s41467-019-12242-1].

1078 107. A. K. Garg et al., “Advances in retinal oximetry,” Transl. Vis. Sci. Technol. **10**(2), 1–
1079 18 (2021) [doi:10.1167/tvst.10.2.5].

1080 108. J. Pichette et al., “Intraoperative video-rate hemodynamic response assessment in
1081 human cortex using snapshot hyperspectral optical imaging,” Neurophotonics **3**(04), 1
1082 (2016) [doi:10.1117/1.nph.3.4.045003].

1083 109. J. M. Kainerstorfer et al., “Quantitative principal component model for skin
1084 chromophore mapping using multi-spectral images and spatial priors,” Biomed. Opt.
1085 Express **2**(5), 1040 (2011) [doi:10.1364/boe.2.001040].

1086 110. K. Kikuchi, Y. Masuda, and T. Hirao, “Imaging of hemoglobin oxygen saturation ratio
1087 in the face by spectral camera and its application to evaluate dark circles,” Ski. Res.
1088 Technol. **19**(4), 499–507 (2013) [doi:10.1111/srt.12074].

1089 111. Q. He and R. Wang, “Hyperspectral imaging enabled by an unmodified smartphone
1090 for analyzing skin morphological features and monitoring hemodynamics,” Biomed.
1091 Opt. Express **11**(2), 895 (2020) [doi:10.1364/boe.378470].

1092 112. E. Zherebtsov et al., “Hyperspectral imaging of human skin aided by artificial neural
1093 networks,” Biomed. Opt. Express **10**(7), 3545 (2019) [doi:10.1364/boe.10.003545].

1094 113. L. C. Cancio, “Application of novel hyperspectral imaging technologies in combat
1095 casualty care,” Emerg. Digit. Micromirror Device Based Syst. Appl. II **7596**(February
1096 2010), 759605 (2010) [doi:10.1117/12.846331].

1097 114. N. T. Clancy et al., “Intraoperative measurement of bowel oxygen saturation using a
1098 multispectral imaging laparoscope,” Biomed. Opt. Express **6**(10), 4179 (2015)

[doi:10.1364/boe.6.004179].

115. T. Pruimboom et al., “Perioperative Hyperspectral Imaging to Assess Mastectomy Skin Flap and DIEP Flap Perfusion in Immediate Autologous Breast Reconstruction: A Pilot Study,” Diagnostics **12**(1) (2022) [doi:10.3390/diagnostics12010184].

116. J. M. Eichenholz et al., “Real-time megapixel multispectral bioimaging,” Imaging, Manip. Anal. Biomol. Cells, Tissues VIII **7568**(February 2010), 75681L (2010) [doi:10.1117/12.842563].

117. A. S. Luthman, *Spectrally Resolved Detector Arrays for Multiplexed Biomedical Fluorescence Imaging*, Springer International Publishing, CHAM (2018) [doi:10.1007/978-3-319-98255-7].

118. S. Grusche, “Basic slit spectroscope reveals three-dimensional scenes through diagonal slices of hyperspectral cubes,” Appl. Opt. **53**(20), 4594 (2014) [doi:10.1364/ao.53.004594].

119. R. Calvini, A. Ulrici, and J. M. Amigo, “Growing applications of hyperspectral and multispectral imaging,” Data Handl. Sci. Technol. **32**, 605–629 (2020) [doi:10.1016/B978-0-444-63977-6.00024-9].

120. T. W. Sawyer, C. Williams, and S. E. Bohndiek, “Spectral band selection and tolerancing for multispectral filter arrays,” Front. Opt. - Proc. Front. Opt. + Laser Sci. APS/DLS(January), 3–5 (2019) [doi:10.1364/FIO.2019.JW4A.126].

121. C. Williams et al., “Grayscale-to-Color: Scalable Fabrication of Custom Multispectral Filter Arrays,” ACS Photonics (2019) [doi:10.1021/acsphotonics.9b01196].

122. R. Wu et al., “Optimized multi-spectral filter arrays for spectral reconstruction,” Sensors (Switzerland) **19**(13) (2019) [doi:10.3390/s19132905].

123. S. Gioux, A. Mazhar, and D. J. Cuccia, “Spatial frequency domain imaging in 2019: principles, applications, and perspectives,” J. Biomed. Opt. **24**(7), 071613 (2019) [doi:10.1117/1].

124. D. J. Cuccia et al., “Quantitation and mapping of tissue optical properties using modulated imaging,” J. Biomed. Opt. **14**(2), 024012 (2009) [doi:10.1117/1.3088140].

125. R. H. Wilson et al., “High-speed spatial frequency domain imaging of rat cortex detects dynamic optical and physiological properties following cardiac arrest and resuscitation,” Neurophotonics **4**(04), 1 (2017) [doi:10.1117/1.nph.4.4.045008].

126. M. T. Ghijsen et al., “Quantitative real-time optical imaging of the tissue metabolic rate of oxygen consumption,” J. Biomed. Opt. **23**(03), 1 (2018) [doi:10.1117/1.jbo.23.3.036013].

127. M. Schmidt et al., “Real-time, wide-field, and quantitative oxygenation imaging using spatiotemporal modulation of light,” J. Biomed. Opt. **24**(07), 1 (2019) [doi:10.1117/1.jbo.24.7.071610].

128. C. Weinkauf et al., “Near-instant noninvasive optical imaging of tissue perfusion for vascular assessment,” J. Vasc. Surg. **69**(2), 555–562, Elsevier Inc. (2019) [doi:10.1016/j.jvs.2018.06.202].

129. S. Jett et al., “Stratification of Microvascular Disease Severity in the Foot Using Spatial Frequency Domain Imaging,” J. Diabetes Sci. Technol. (2021)

[doi:10.1177/19322968211024666].

130. A. Ponticorvo et al., “Spatial Frequency Domain Imaging (SFDI) of clinical burns: A case report,” Burn. Open **4**(2), 67–71, The Authors (2020) [doi:10.1016/j.burnso.2020.02.004].

131. J. Sun et al., “ Enhancing in vivo tumor boundary delineation with structured illumination fluorescence molecular imaging and spatial gradient mapping ,” J. Biomed. Opt. **21**(8), 080502 (2016) [doi:10.1117/1.jbo.21.8.080502].

132. D. Wirth et al., “Feasibility of using spatial frequency-domain imaging intraoperatively during tumor resection,” J. Biomed. Opt. **24**(07), 1 (2018) [doi:10.1117/1.jbo.24.7.071608].

133. P. A. Valdes et al., “qF-SSOP: real-time optical property corrected fluorescence imaging,” Biomed. Opt. Express **8**(8), 3597 (2017) [doi:10.1364/boe.8.003597].

134. Y. Garini, I. T. Young, and G. McNamara, “Spectral imaging: Principles and applications,” Cytom. Part A **69**(8), 735–747 (2006) [doi:10.1002/cyto.a.20311].

135. J. Wei and X. Wang, “An Overview on Linear Unmixing of Hyperspectral Data,” Math. Probl. Eng. **2020** (2020) [doi:10.1155/2020/3735403].

136. M. D. Mura, J. Chanussot, and A. Plaza, “An overview on Hyperspectral Unmixing,” GIPSA-Lab, Grenoble Inst. Techonology (2014).

137. J. S. Bhatt and M. V. Joshi, “Deep Learning in Hyperspectral Unmixing: A Review,” Int. Geosci. Remote Sens. Symp., 2189–2192 (2020) [doi:10.1109/IGARSS39084.2020.9324546].

138. A. Grigoroiu, J. Yoon, and S. E. Bohndiek, “Deep learning applied to hyperspectral endoscopy for online spectral classification,” Sci. Rep. **10**(1), 1–10, Springer US (2020) [doi:10.1038/s41598-020-60574-6].

139. S. Li et al., “Deep learning for hyperspectral image classification: An overview,” IEEE Trans. Geosci. Remote Sens. **57**(9), 6690–6709 (2019) [doi:10.1109/TGRS.2019.2907932].

140. J. Gröhl et al., “Learned spectral decoloring enables photoacoustic oximetry,” Sci. Rep. **11**(1), 1–12, Nature Publishing Group UK (2021) [doi:10.1038/s41598-021-83405-8].

141. L. Lin et al., “Single-breath-hold photoacoustic computed tomography of the breast,” Nat. Commun. **9**(1) (2018) [doi:10.1038/s41467-018-04576-z].

142. M. Li, Y. Tang, and J. Yao, “Photoacoustic tomography of blood oxygenation: A mini review,” Photoacoustics **10**(December 2017), 65–73 (2018) [doi:10.1016/j.pacs.2018.05.001].

143. J. Jo et al., “A Functional Study of Human Inflammatory Arthritis Using Photoacoustic Imaging,” Sci. Rep. **7**(1), 1–9 (2017) [doi:10.1038/s41598-017-15147-5].

144. N. C. Biswal, Y. Xu, and Q. Zhu, “Imaging tumor oxyhemoglobin and deoxyhemoglobin concentrations with ultrasound-guided diffuse optical tomography,” Technol. Cancer Res. Treat. **10**(5), 417–429 (2011) [doi:10.7785/tcrt.2012.500219].

145. D. Orive-Miguel et al., “Real-time dual-wavelength time-resolved diffuse optical tomography system for functional brain imaging based on probe-hosted silicon

photomultipliers," Sensors (Switzerland) **20**(10) (2020) [doi:10.3390/s20102815].

146. Y. Wang et al., "Combined diffuse optical tomography and photoacoustic tomography for enhanced functional imaging of small animals: a methodological study on phantoms," Appl. Opt. **56**(2), 303 (2017) [doi:10.1364/ao.56.000303].

147. S. Agrawal et al., "Functional, molecular and structural imaging using LED-based photoacoustic and ultrasound imaging system.," SPIE BiOS(February 2020), 188 (2020) [doi:10.1117/12.2547048].

148. D. Lighter et al., "Multispectral, non-contact diffuse optical tomography of healthy human finger joints," Biomed. Opt. Express **9**(4), 1445 (2018) [doi:10.1364/boe.9.001445].

149. S. P. Chong et al., "Cerebral metabolic rate of oxygen (CMRO_2) assessed by combined Doppler and spectroscopic OCT," Biomed. Opt. Express **6**(10), 3941 (2015) [doi:10.1364/boe.6.003941].

150. E. Brown, J. Brunker, and S. E. Bohndiek, "Photoacoustic imaging as a tool to probe the tumour microenvironment," DMM Dis. Model. Mech. **12**(7) (2019) [doi:10.1242/dmm.039636].

151. I. Steinberg et al., "Photoacoustic clinical imaging," Photoacoustics **14**(September 2018), 77–98, Elsevier (2019) [doi:10.1016/j.pacs.2019.05.001].

152. E. I. Neuschler et al., "BREAST IMAGING: Optoacoustic Imaging to Diagnose Benign and Malignant Breast Masses Neuschler et al Materials and Methods," Radiology **287**(2) (2017) [doi:10.1148/radiol.2017172228].

153. S. Manohar and M. Dantuma, “Current and future trends in photoacoustic breast imaging,” Photoacoustics **16**(September 2018), 100134, Elsevier (2019) [doi:10.1016/j.pacs.2019.04.004].

154. M. Omar, J. Aguirre, and V. Ntziachristos, “Optoacoustic mesoscopy for biomedicine,” Nat. Biomed. Eng. **3**(5), 354–370, Springer US (2019) [doi:10.1038/s41551-019-0377-4].

155. G. L. G. Menezes et al., “Downgrading of breast masses suspicious for cancer by using optoacoustic breast imaging,” Radiology **288**(2), 355–365 (2018) [doi:10.1148/radiol.2018170500].

156. W. Roll et al., “Multispectral optoacoustic tomography of benign and malignant thyroid disorders: A pilot study,” J. Nucl. Med. **60**(10), 1461–1466 (2019) [doi:10.2967/jnumed.118.222174].

157. S. Zackrisson, S. M. W. Y. Van De Ven, and S. S. Gambhir, “Light in and sound out: Emerging translational strategies for photoacoustic imaging,” Cancer Res. **74**(4), 979–1004 (2014) [doi:10.1158/0008-5472.CAN-13-2387].

158. P. K. Upputuri and M. Pramanik, “Recent advances toward preclinical and clinical translation of photoacoustic tomography: a review,” J. Biomed. Opt. **22**(4), 041006 (2016) [doi:10.1117/1.jbo.22.4.041006].

159. W. C. Chapman and M. Mutch, “Co-registered photoacoustic and ultrasound imaging of human colorectal cancer,” J. Biomed. Opt. **24**(12), 1 (2019) [doi:10.1117/1.jbo.24.12.121913].

160. G. S. Sangha and C. J. Goergen, “Label-free photoacoustic and ultrasound imaging for murine atherosclerosis characterization,” APL Bioeng. **4**(2), 026102, AIP Publishing LLC (2020) [doi:10.1063/1.5142728].

161. Y. Wang et al., “A portable three-dimensional photoacoustic tomography system for imaging of chronic foot ulcers,” Quant. Imaging Med. Surg. **9**(5), 799–806 (2019) [doi:10.21037/qims.2019.05.02].

162. F. Knieling et al., “Multispectral Optoacoustic Tomography for Assessment of Crohn’s Disease Activity,” N. Engl. J. Med. **376**(13), 2016–2017 (2017) [doi:10.1056/NEJMc1612455].

163. V. Ntziachristos and D. Razansky, “Molecular imaging by means of multispectral optoacoustic tomography (MSOT),” Chem. Rev. **110**(5), 2783–2794 (2010) [doi:10.1021/cr9002566].

164. E. Maneas et al., “Photoacoustic imaging of the human placental vasculature,” J. Biophotonics **13**(4), 1–10 (2020) [doi:10.1002/jbio.201900167].

165. T. Shiina, M. Toi, and T. Yagi, “Development and clinical translation of photoacoustic mammography,” Biomed. Eng. Lett. **8**(2), 157–165, The Korean Society of Medical and Biological Engineering (2018) [doi:10.1007/s13534-018-0070-7].

166. P. G. Anderson et al., “Broadband optical mammography: Chromophore concentration and hemoglobin saturation contrast in breast cancer,” PLoS One **10**(3), 1–23 (2015) [doi:10.1371/journal.pone.0117322].

167. L. He et al., “Noncontact diffuse correlation tomography of human breast tumor,” J.

Biomed. Opt. **20**(8), 086003 (2015) [doi:10.1117/1.jbo.20.8.086003].

168. M. Erfanzadeh and Q. Zhu, “Photoacoustic imaging with low-cost sources; A review,” Photoacoustics **14**(December 2018), 1–11, Elsevier (2019) [doi:10.1016/j.pacs.2019.01.004].

169. D. Das et al., “Another decade of photoacoustic imaging,” Phys. Med. Biol. **66**(5), IOP Publishing (2021) [doi:10.1088/1361-6560/abd669].

170. A. B. E. Attia et al., “A review of clinical photoacoustic imaging: Current and future trends,” Photoacoustics **16**(July), 100144, Elsevier (2019) [doi:10.1016/j.pacs.2019.100144].

171. M. Xu and L. V. Wang, “Photoacoustic imaging in biomedicine,” Rev. Sci. Instrum. **77**(4) (2006) [doi:10.1063/1.2195024].

172. P. Beard, “Biomedical photoacoustic imaging,” Interface Focus **1**(4), 602–631 (2011) [doi:10.1098/rsfs.2011.0028].

173. B. T. Cox, J. G. Laufer, and P. C. Beard, “Quantitative Photoacoustic Image Reconstruction using Fluence Dependent Chromophores,” Biomed. Opt. Express **1**(1), 201 (2010) [doi:10.1364/boe.1.000201].

174. S. Bohndiek, “Addressing photoacoustics standards,” Nat. Photonics **13**(5), 298, Springer US (2019) [doi:10.1038/s41566-019-0417-3].

175. H. Singh et al., “Mapping cortical haemodynamics during neonatal seizures using diffuse optical tomography: A case study,” NeuroImage Clin. **5**, 256–265, Elsevier B.V. (2014) [doi:10.1016/j.nicl.2014.06.012].

176. M. D. Wheelock, J. P. Culver, and A. T. Eggebrecht, “High-density diffuse optical tomography for imaging human brain function,” Rev. Sci. Instrum. **90**(5) (2019) [doi:10.1063/1.5086809].

177. Y. Hoshi and Y. Yamada, “Overview of diffuse optical tomography and its clinical applications,” J. Biomed. Opt. **21**(9), 091312 (2016) [doi:10.1117/1.jbo.21.9.091312].

178. A. P. Gibson, J. C. Hebden, and S. R. Arridge, “Recent advances in diffuse optical imaging,” Phys. Med. Biol. **50**(4) (2005) [doi:10.1088/0031-9155/50/4/R01].

179. W. Zhi et al., “Predicting Treatment Response of Breast Cancer to Neoadjuvant Chemotherapy Using Ultrasound-Guided Diffuse Optical Tomography,” Transl. Oncol. **11**(1), 56–64, The Authors (2018) [doi:10.1016/j.tranon.2017.10.011].

180. R. Choe and T. Durduran, “Diffuse Optical Monitoring of the Neoadjuvant Breast Cancer Therapy,” IEEE J. Sel. Top. Quantum Electron. **18**(4), 1367–1386 (2012) [doi:10.1109/JSTQE.2011.2177963].

181. F. Scholkmann et al., “A review on continuous wave functional near-infrared spectroscopy and imaging instrumentation and methodology,” Neuroimage **85**, 6–27, Elsevier Inc. (2014) [doi:10.1016/j.neuroimage.2013.05.004].

182. K. A. S. Mithun and W. Xia, “Portable and Affordable Light Source-Based Photoacoustic Tomography,” Sensors **20**(6173) (2020) [doi:10.3390/s20216173].

183. V. V. Beschastnov et al., “Current methods for the assessment of oxygen status and biotissue microcirculation condition: Diffuse optical spectroscopy (review),” Sovrem. Tehnol. v Med. **10**(4), 183–194 (2018) [doi:10.17691/stm2018.10.4.22].

184. A. Curtin et al., “A systematic review of integrated functional near-infrared spectroscopy (fNIRS) and transcranial magnetic stimulation (TMS) studies,” Front. Neurosci. **13**(FEB) (2019) [doi:10.3389/fnins.2019.00084].

185. P. Pinti et al., “The present and future use of functional near-infrared spectroscopy (fNIRS) for cognitive neuroscience,” Ann. N. Y. Acad. Sci. **1464**, 5–29 (2018) [doi:10.1111/nyas.13948].

186. A. Pifferi et al., “New frontiers in time-domain diffuse optics, a review,” J. Biomed. Opt. **21**(9), 091310 (2016) [doi:10.1117/1.jbo.21.9.091310].

187. E. E. Vidal-Rosas et al., “Evaluating a new generation of wearable high-density diffuse optical tomography technology via retinotopic mapping of the adult visual cortex,” Neurophotonics **8**(2), 1–24 (2021) [doi:10.1117/1.NPh.8.2.025002].

188. G. Di Leo et al., “Optical imaging of the breast: Basic principles and clinical applications,” Am. J. Roentgenol. **209**(1), 230–238 (2017) [doi:10.2214/AJR.16.17220].

189. F. Y. Wong et al., “Impaired autoregulation in preterm infants identified by using spatially resolved spectroscopy,” Pediatrics **121**(3) (2008) [doi:10.1542/peds.2007-1487].

190. Y. Shang, T. Li, and G. Yu, “Clinical applications of near-infrared diffuse correlation spectroscopy and tomography for tissue blood flow monitoring and imaging,” Physiol. Meas. **38**(4), R1–R26 (2017) [doi:10.1088/1361-6579/aa60b7].

191. H. S. Yazdi et al., “Mapping breast cancer blood flow index, composition, and

metabolism in a human subject using combined diffuse optical spectroscopic imaging and diffuse correlation spectroscopy," J. Biomed. Opt. **22**(4), 045003 (2017) [doi:10.1117/1.jbo.22.4.045003].

192. I. Fredriksson and M. Larsson, "On the equivalence and differences between laser Doppler flowmetry and laser speckle contrast analysis," J. Biomed. Opt. **21**(12), 126018 (2016) [doi:10.1117/1.jbo.21.12.126018].

193. H. Jonasson et al., "Oxygen saturation, red blood cell tissue fraction and speed resolved perfusion - A new optical method for microcirculatory assessment," Microvasc. Res. **102**, 70–77, Elsevier B.V. (2015) [doi:10.1016/j.mvr.2015.08.006].

194. W. Heeman et al., "Clinical applications of laser speckle contrast imaging: a review," J. Biomed. Opt. **24**(08), 1 (2019) [doi:10.1117/1.jbo.24.8.080901].

195. Q. Fang and S. Yan, "MCX Cloud—a modern, scalable, high-performance and in-browser Monte Carlo simulation platform with cloud computing," J. Biomed. Opt. **27**(08), 1–14 (2022) [doi:10.1117/1.jbo.27.8.083008].

196. S. R. P. K. Lanka et al., "A multi-laboratory comparison of photon migration instruments and their performances: the BitMap exercise," 11 (2021) [doi:10.1117/12.2578521].

197. L. Di Sieno et al., "Solid heterogeneous phantoms for multimodal ultrasound and diffuse optical imaging: an outcome of the SOLUS project for standardization," 39 (2019) [doi:10.1117/12.2526645].

198. L. Kagemann et al., "Spectral oximetry assessed with high-speed ultra-high- resolution

optical coherence tomography Larry," J. Biomed. Opt. **12**(4), 1–19 (2007) [doi:10.1117/1.2772655.Spectral].

199. J. Yi and X. Li, "Estimation of oxygen saturation from erythrocytes by high-resolution spectroscopic optical coherence tomography," Opt. Lett. **35**(12), 2094 (2010) [doi:10.1364/ol.35.002094].

200. F. E. Robles, S. Chowdhury, and A. Wax, "Assessing hemoglobin concentration using spectroscopic optical coherence tomography for feasibility of tissue diagnostics.," Biomed. Opt. Express **1**(1), 310–317 (2010) [doi:10.1364/boe.1.000310/].

201. J. A. Winkelmann et al., "Spectral contrast optical coherence tomography angiography enables single-scan vessel imaging," Light Sci. Appl. **8**(1), Springer US (2019) [doi:10.1038/s41377-018-0117-7].

202. M. J. Casper et al., "Capillary Refill—The Key to Assessing Dermal Capillary Capacity and Pathology in Optical Coherence Tomography Angiography," Lasers Surg. Med. **52**(7), 653–658 (2020) [doi:10.1002/lsm.23188].

203. S. Pi et al., "Retinal capillary oximetry with visible light optical coherence tomography," Proc. Natl. Acad. Sci. U. S. A. **117**(21) (2020) [doi:10.1073/pnas.1918546117].

204. A. H. Kashani et al., "Optical coherence tomography angiography: A comprehensive review of current methods and clinical applications," Prog. Retin. Eye Res. **60**, 66–100, Elsevier Ltd (2017) [doi:10.1016/j.preteyeres.2017.07.002].

205. M. Liu and W. Drexler, "Optical coherence tomography angiography and

photoacoustic imaging in dermatology," Photochem. Photobiol. Sci. **18**(5), 945–962, Royal Society of Chemistry (2019) [doi:10.1039/c8pp00471d].

206. S. Chen et al., "Retinal oximetry in humans using visible-light optical coherence tomography [Invited]," Biomed. Opt. Express **8**(3), 1415 (2017) [doi:10.1364/boe.8.001415].

207. W. Song et al., "Visible light optical coherence tomography angiography (vis-OCTA) facilitates local microvascular oximetry in the human retina," Biomed. Opt. Express **11**(7), 4037 (2020) [doi:10.1364/boe.395843].

208. D. Huang et al., "Optical coherence tomography," in Science **254**(5035), pp. 1178–1181 (1991) [doi:10.1126/science.1957169].

209. R. Leitgeb, C. K. Hitzenberger, and A. F. Fercher, "Performance of fourier domain vs. time domain optical coherence tomography.," Opt. Express **11**(8), 889–894 (2003).

210. B. Povazay et al., "Visible light optical coherence tomography," Coherence Domain Opt. Methods Biomed. Sci. Clin. Appl. VI **4619**(June 2002), 90 (2002) [doi:10.1117/12.470466].

211. S. P. Chong et al., "Quantitative microvascular hemoglobin mapping using visible light spectroscopic Optical Coherence Tomography," Biomed. Opt. Express **6**(4), 1429 (2015) [doi:10.1364/boe.6.001429].

212. J. Yi et al., "Visible-light optical coherence tomography for retinal oximetry.," Opt. Lett. **38**(11), 1796–1798 (2013) [doi:10.1364/OL.38.001796].

213. S. Chen, J. Yi, and H. F. Zhang, "Measuring oxygen saturation in retinal and choroidal

circulations in rats using visible light optical coherence tomography angiography," Biomed. Opt. Express **6**(8), 2840 (2015) [doi:10.1364/BOE.6.002840].

214. G. J. Tearney et al., "In vivo Endoscopic Optical Biopsy with Optical Coherence Tomography," Science (80-.). **276**(5321), 2037–2039 (1997).

215. B. C. Quirk et al., "In situ imaging of lung alveoli with an optical coherence tomography needle probe.," J. Biomed. Opt. **16**(3), 036009 (2011) [doi:10.1117/1.3556719].

216. H. Yabushita et al., "Characterization of human atherosclerosis by optical coherence tomography," Circulation **106**(13), 1640–1645 (2002) [doi:10.1161/01.CIR.0000029927.92825.F6].

217. J. A. Evans et al., "Optical coherence tomography to identify intramucosal carcinoma and high-grade dysplasia in Barrett's esophagus," Clin. Gastroenterol. Hepatol. **4**(1), 38–43 (2006) [doi:10.1016/S1542-3565(05)00746-9].

218. D. Lorenser, R. A. Mclaughlin, and D. D. Sampson, *Optical Coherence Tomography in a Needle Format*, 2015th ed., in Optical Coherence Tomography, 2015th ed., W. Drexler and J. G. Fujimoto, Eds., Springer, Switzerland (2015) [doi:10.1007/978-3-319-06419-2].

219. S. Song, J. Xu, and R. K. Wang, "Long-range and wide field of view optical coherence tomography for in vivo 3D imaging of large volume object based on akinetic programmable swept source," Biomed. Opt. Express **7**(11), 4734 (2016) [doi:10.1364/boe.7.004734].

220. M. Ulrich et al., “Dynamic Optical Coherence Tomography in Dermatology,” Dermatology **232**(3), 298–311 (2016) [doi:10.1159/000444706].

221. H. Liang et al., “Optical coherence tomography for art conservation and archaeology,” O3A Opt. Arts, Archit. Archaeol. **6618**(May 2014), 661805 (2007) [doi:10.1117/12.726032].

222. W. Kang et al., “Optical Coherence Tomography for Gastrointestinal Endoscopy,” in Optical Coherence Tomography Technology and Applications Second Edition, pp. 2051–2076 (2015).

223. G. J. Tearney et al., “Imaging Coronary Atherosclerosis and Vulnerable Plaques with Optical Coherence Tomography,” in Optical Coherence Tomography Technology and Applications Second Edition, pp. 2109–2130 (2015).

224. K. Liang et al., “Tethered capsule en face optical coherence tomography for imaging Barrett’s oesophagus in unsedated patients,” BMJ Open Gastroenterol. **7**(1), 1–8 (2020) [doi:10.1136/bmjgast-2020-000444].

225. M. V. Volkov et al., “Video capillaroscopy clarifies mechanism of the photoplethysmographic waveform appearance,” Sci. Rep. **7**(1), 1–8 (2017) [doi:10.1038/s41598-017-13552-4].

226. J. Aguirre et al., “Assessing nailfold microvascular structure with ultra-wideband raster-scan optoacoustic mesoscopy,” Photoacoustics **10**, 31–37, Elsevier GmbH. (2018) [doi:10.1016/j.pacs.2018.02.002].

227. A. K. Murray et al., “Noninvasive imaging techniques in the assessment of

scleroderma spectrum disorders," Arthritis Care Res. **61**(8), 1103–1111 (2009) [doi:10.1002/art.24645].

228. A. Karbalaie et al., "Practical issues in assessing nailfold capillaroscopic images: a summary," Clin. Rheumatol. **38**(9), 2343–2354, Clinical Rheumatology (2019) [doi:10.1007/s10067-019-04644-9].

229. D. Paxton and J. D. Pauling, "Does nailfold capillaroscopy help predict future outcomes in systemic sclerosis? A systematic literature review," Semin. Arthritis Rheum. **48**(3), 482–494, Elsevier Inc. (2018) [doi:10.1016/j.semarthrit.2018.02.005].

230. M. Berks et al., "An automated system for detecting and measuring nailfold capillaries," Lect. Notes Comput. Sci. (including Subser. Lect. Notes Artif. Intell. Lect. Notes Bioinformatics) **8673 LNCS**(PART 1), 658–665 (2014) [doi:10.1007/978-3-319-10404-1_82].

231. M. E. Anderson et al., "Computerized nailfold video capillaroscopy - A new tool for assessment of Raynaud's phenomenon," J. Rheumatol. **32**(5), 841–848 (2005).

232. G. N. McKay, N. Mohan, and N. J. Durr, "Imaging human blood cells in vivo with oblique back-illumination capillaroscopy," Biomed. Opt. Express **11**(5), 2373 (2020) [doi:10.1364/boe.389088].

233. M. Michalska-Jakubus et al., "Plasma endothelial microparticles reflect the extent of capillaroscopic alterations and correlate with the severity of skin involvement in systemic sclerosis," Microvasc. Res. **110**, 24–31 (2017) [doi:10.1016/j.mvr.2016.11.006].

234. B. Ruaro et al., “Correlations between skin blood perfusion values and nailfold capillaroscopy scores in systemic sclerosis patients,” Microvasc. Res. **105**, 119–124, Elsevier B.V. (2016) [doi:10.1016/j.mvr.2016.02.007].

235. M. Ewerlöf, M. Larsson, and E. G. Salerud, “Spatial and temporal skin blood volume and saturation estimation using a multispectral snapshot imaging camera,” Imaging, Manip. Anal. Biomol. Cells, Tissues XV **10068**(February 2017), 1006814 (2017) [doi:10.1117/12.2251928].

236. N. Hagen and M. W. Kudenov, “Review of snapshot spectral imaging technologies,” Opt. Eng. **52**(9), 090901 (2013) [doi:10.1117/1.oe.52.9.090901].

237. M. Torabzadeh et al., “Hyperspectral imaging in the spatial frequency domain with a supercontinuum source,” J. Biomed. Opt. **24**(07), 1 (2019) [doi:10.1117/1.jbo.24.7.071614].

238. M. A. Wares et al., “Noninvasive evaluation of hemodynamics and light scattering property during two-stage mouse cutaneous carcinogenesis based on multispectral diffuse reflectance images at isosbestic wavelengths of hemoglobin,” J. Biomed. Opt. **24**(03), 1 (2019) [doi:10.1117/1.jbo.24.3.031020].

239. D. J. Waterhouse et al., “Emerging optical methods for endoscopic surveillance of Barrett’s oesophagus,” Lancet Gastroenterol. Hepatol. **3**(5), 349–362, Elsevier Ltd (2018) [doi:10.1016/S2468-1253(18)30030-X].

240. T. Chiba et al., “Advanced multispectral image-processing endoscopy system for visualizing two-dimensional hemoglobin saturation and relative hemoglobin concentration,” Endosc. Int. Open **07**(11), E1442–E1447 (2019) [doi:10.1055/a-0990-

9189].

241. G. Ku et al., “Multiple-bandwidth photoacoustic tomography,” Phys. Med. Biol. **49**(7), 1329–1338 (2004) [doi:10.1088/0031-9155/49/7/018].

242. T. P. Nguyen et al., “Improved depth-of-field photoacoustic microscopy with a multifocal point transducer for biomedical imaging,” Sensors (Switzerland) **20**(7), 1–18 (2020) [doi:10.3390/s20072020].

243. C. Chu et al., “Multimodal Photoacoustic Imaging-Guided Regression of Corneal Neovascularization: A Non-Invasive and Safe Strategy,” Adv. Sci. **2000346**, 1–7 (2020) [doi:10.1002/advs.202000346].

244. M. Martinho Costa et al., “Quantitative photoacoustic imaging study of tumours in vivo: Baseline variations in quantitative measurements,” Photoacoustics **13**(May 2018), 53–65, Elsevier (2019) [doi:10.1016/j.pacs.2018.12.002].

245. P. Zhang et al., “High-resolution deep functional imaging of the whole mouse brain by photoacoustic computed tomography in vivo,” J. Biophotonics **11**(1), 1–6 (2018) [doi:10.1002/jbio.201700024].

246. R. Haindl et al., “Functional optical coherence tomography and photoacoustic microscopy imaging for zebrafish larvae,” Biomed. Opt. Express **11**(4), 2137 (2020) [doi:10.1364/boe.390410].

247. H. Leng et al., “Characterization of a fiber bundle-based real-time ultrasound/photoacoustic imaging system and its in vivo functional imaging applications,” Micromachines **10**(12) (2019) [doi:10.3390/mi10120820].

248. A. Hariri et al., “The characterization of an economic and portable LED-based photoacoustic imaging system to facilitate molecular imaging,” Photoacoustics **9**, 10–20, Elsevier GmbH. (2018) [doi:10.1016/j.pacs.2017.11.001].

249. Y. Junjie et al., “High-speed Label-free Functional Photoacoustic Microscopy of Mouse Brain in Action,” Nat. Methods **12**(4), 407–410 (2015) [doi:doi:10.1038/nmeth.3336].

250. H. F. Zhang et al., “Functional photoacoustic microscopy for high-resolution and noninvasive in vivo imaging,” Nat. Biotechnol. **24**(7), 848–851 (2006) [doi:10.1038/nbt1220].

251. A. Taruttis and V. Ntziachristos, “Advances in real-time multispectral optoacoustic imaging and its applications,” Nat. Photonics **9**(4), 219–227, Nature Publishing Group (2015) [doi:10.1038/nphoton.2015.29].

252. S. Chen et al., “Imaging hemodynamic response after ischemic stroke in mouse cortex using visible-light optical coherence tomography,” Biomed. Opt. Express **7**(9), 3377 (2016) [doi:10.1364/BOE.7.003377].

253. P. L. Nesper et al., “OCT angiography and visible-light OCT in diabetic retinopathy,” Vision Res. **139**, 191–203, Elsevier Ltd (2017) [doi:10.1016/j.visres.2017.05.006].

254. S. Pi et al., “Automated spectroscopic retinal oximetry with visible-light optical coherence tomography,” Biomed. Opt. Express **9**(5), 2056 (2018) [doi:10.1364/boe.9.002056].

255. B. T. Soetikno et al., “Inner retinal oxygen metabolism in the 50/10 oxygen-induced

retinopathy model," Sci. Rep. **5**, 16752 (2015) [doi:10.1038/srep16752].

256. W. Liu et al., "Increased retinal oxygen metabolism precedes microvascular alterations in type 1 diabetic mice," Investig. Ophthalmol. Vis. Sci. **58**(2), 981–989 (2017) [doi:10.1167/iovs.16-20600].

257. F. Picot et al., "Interstitial imaging with multiple diffusive reflectance spectroscopy projections for in vivo blood vessels detection during brain needle biopsy procedures," Neurophotonics **6**(02), 1 (2019) [doi:10.1117/1.nph.6.2.025003].

258. V. C. Kavuri et al., "Sparsity enhanced spatial resolution and depth localization in diffuse optical tomography," 13695–13708 (2012).

259. R. Baikejiang, W. Zhang, and C. Li, "Diffuse optical tomography for breast cancer imaging guided by computed tomography: A feasibility study," J. Xray. Sci. Technol. **25**(3), 341–355 (2017) [doi:10.3233/XST-16183].

260. S. Brigadoi et al., "A 4D neonatal head model for diffuse optical imaging of pre-term to term infants," Neuroimage **100**, 385–394, Elsevier Inc. (2014) [doi:10.1016/j.neuroimage.2014.06.028].

261. M. A. Khalil et al., "Dynamic diffuse optical tomography imaging of peripheral arterial disease," Biomed. Opt. Express **3**(9), 2288 (2012) [doi:10.1364/boe.3.002288].

262. D. A. Boas et al., "Establishing the diffuse correlation spectroscopy signal relationship with blood flow," Neurophotonics **3**(3), 031412 (2016) [doi:10.1117/1.nph.3.3.031412].

263. Z. Hosseinaee, J. A. Tummon Simmons, and P. H. Reza, "Dual-Modal Photoacoustic

Imaging and Optical Coherence Tomography [Review],” Front. Phys. **8**(January), 1–19 (2021) [doi:10.3389/fphy.2020.616618].

264. H. Jonasson et al., “Validation of speed-resolved laser Doppler perfusion in a multimodal optical system using a blood-flow phantom,” J. Biomed. Opt. **24**(09), 1 (2019) [doi:10.1117/1.jbo.24.9.095002].

265. K. F. Ma et al., “Laser Doppler Flowmetry Combined with Spectroscopy to Determine Peripheral Tissue Perfusion and Oxygen Saturation : A Pilot Study in Healthy Volunteers and Patients with Peripheral Arterial Disease” (2022).

266. G. Wang et al., “Impact of local thermal stimulation on the correlation between oxygen saturation and speed-resolved blood perfusion,” Sci. Rep. **10**(1), 1–10, Springer US (2020) [doi:10.1038/s41598-019-57067-6].

267. A. Pellicer et al., “The SafeBoosC phase II randomised clinical trial: A treatment guideline for targeted near-infrared-derived cerebral tissue oxygenation versus standard treatment in extremely preterm infants,” Neonatology **104**(3), 171–178 (2013) [doi:10.1159/000351346].